PHYSICAL SOCIETY OF LONDON.

MEMOIRS

OF THE

COLLEGE OF SCIENCE

KYOTO IMPERIAL UNIVERSITY

SERIES A

VOL. XV, NO. 2

MARCH 1932

KYOTO

On the Origin of the X-Ray Non-Diagram Lines in the *K* Series

By

Masao Sawada

(Received November 21, 1931)

Abstract

To establish a scheme for the X-ray non-diagram lines (frequently called "spark lines" or "satellites"), the author assumed two-electron jumps in a doubly-ionized atom, obeying the Heisenberg selection rule for the quantum number l. The $\frac{\nu}{R}$-values were computed by this hypothesis and compared with the experimental data.

The results arrived at, which seem to account for the origin of these lines, are:

Origin		Non-diagram line	Origin		Non-diagram line
Initial state	Final state		Initial state	Final state	
KL_{I}	$L_{\mathrm{I}}\,M_{\mathrm{II,III}}$	$K\beta'''$	KM_{I}	$M_{\mathrm{I}}\,M_{\mathrm{II,III}}$	$K\beta''$
$KL_{\mathrm{II,III}}$	$L_{\mathrm{II,III}}\,M_{\mathrm{II,III}}$	$K\beta'''$	$KL_{\mathrm{II,III}}$	$L_{\mathrm{I}}\,M_{\mathrm{IV,V}}$	$K\beta'$ (or $K\beta_3$)
$KM_{\mathrm{II,III}}$	$M_{\mathrm{I}}\,M_{\mathrm{IV,V}}$	$K\beta''$	$KL_{\mathrm{II,III}}$	$L_{\mathrm{I}}\,M_{\mathrm{I}}$	$K\beta\eta$ (or $K\beta_4$)

The intensity of these lines, except that of $K\beta''$, was estimated from the experimental values of the lines of the L series, and found in close agreement qualitatively.

The term multiplicities, and the effect of chemical combination are also discussed. It is of interest to notice that the scheme of the non-diagram lines $K\alpha'$, α_3, α_4, α_5, α_6, etc. can be included in $KL_{\mathrm{I}}-L_{\mathrm{I}}L_{\mathrm{II,III}}$ and $KL_{\mathrm{II,III}}-L^2_{\mathrm{II,III}}$, by the experimental rules of the transition probability obtained in this paper, although the author cannot calculate the $\frac{\nu}{R}$-values in the case of the $\{LS\}$ coupling. Hence the result of Langer concerning the origin of the non-diagram line of the $K\alpha$ group was included in the present scheme.

Introduction

In the X-ray emission spectra of an atom, there are a number of faint lines which do not belong to the so-called "*diagram lines*".

It is obvious that the " diagram lines " are produced by transitions between ionized states in which one electron is missing from one of the $K, L, M, \ldots\ldots$levels, and follows the Moseley law.

We call an X-ray emission line, whose frequency cannot be *directly* derived from the well-known system of X-ray absorption levels, a " *non-diagram line* ".

The non-diagram lines are frequently called " *satellites* ", since apparently they accompany an intense diagram line, although this is not always the case; or " *spark lines* ", since Wentzel[1] suggested that the non-diagram lines might originate from a multiply-ionized atom in the inner electron shells.

The characteristic features of these lines are broad and diffuse, and it has been verified that these lines consist of unresolved components by many authors.

In the K series there are α', α_3, α_4, α_5, α_6, as the $K\alpha$- satellites, and β', β'', β''', as the $K\beta$-satellites[2].

Recently H. Beuthe[3] has obtained the new non-diagram lines $\beta\gamma$ and $\beta\eta$, according to his terminology, in many elements between Y (39) and V(23). The line $\beta\gamma$ of Beuthe is the same as the line β''', or seems to be the continuation of it. This point has been discussed by S. Kawata[4] and G. B. Deodhar[5].

The present writer[6] also obtained similar lines to $\beta\eta$ in some other elements.

In this paper the origin of the non-diagram lines of the $K\beta$ series will be treated in detail.

In Table I are collected the $\frac{\nu}{R}$-value of the non-diagram lines measured by many investigators[7]. Many of them are computed from

1. G. Wentzel, Ann. d. Phys. **66**, 437 (1921).
2. Handb. d. Experimentalphysik **24**, **2**, 236 (1930).
3. H. Beuthe, ZS. f. Phys. **60**, 603 (1930).
4. S. Kawata, Mem. Coll. Sci. Kyoto Imp. Univ. (**A**) **13**, 383 (1930).
5. G. B. Deodhar, Roy. Soc. Proc. (**A**) **131**, 633 (1931).
6. M. Sawada, a paper in course of publication.
7. E. Hjalmar, ZS. f. Phys. **1**, 439 (1920); **7**, 341 (1921); Phil. Mag. **41**, 675 (1921).
   V. Dolejšek, C. R. **174**, 411 (1922).
   V. Dolejšek and M. Siegbahn, ZS. f. Phys. **10**, 159 (1922).
   T. Wetterblad, ZS. f. Phys. **42**, 611 (1927); **49**, 670 (1928).
   M. J. Druyvesteyn, ZS. f. Phys. **43**, 707 (1927); Dissertation, Groningen (1928).
   S. Eriksson, ZS. f. Phys. **48**, 360 (1928).
   S. v. Friesen, ZS. f. Phys. **58**, 781 (1929).
   H. Beuthe, ZS. f. Phys. **60**, 603 (1930).
   S. Kawata, *loc. cit.*

their wave-lengths by the present writer, use being made of the relation:

$$\log \frac{\nu}{R} = 5.9596469 - \log \lambda.$$

Table I

The $\frac{\nu}{R}$-values of the non-diagram lines in the $K\beta$ group measured by Hjalmar (H.), Dolejšek (D.), Dolejšek and Siegbahn (D.–S.), Wetterblad (W.), Druyvesteyn (Dr.), Eriksson (E.), Friesen (F.), Beuthe (B.) and Kawata (K.)

Element	β''' ($\beta\gamma$)	β''	β'	β_3	$\beta\eta$
11 Na	—	—	—	77.873 W.	—
12 Mg	—	—	—	94.46 H.W.	—
13 Al	116.55 116.99 Dr.	—	—	113.55 H. 113.31 W.	—
14 Si	137.28 137.95 Dr.	—	—	134.14 H.	—
15 P	159.87 160.46 Dr.	—	—	156.57 D.H.	—
16 S	184.45 Dr.	—	—	180.64 D. 180.56 H.	—
17 Cl	210.63 Dr.	—	—	206.82 D.	—
19 K	267.97 Dr. 267.67 268.31 W.	264.67 Dr. 264.71 H.	—	—	—
20 Ca	299.33 Dr. 299.01 299.75 W.	295.90 Dr. 295.95 H.	294.80 D.–S.	—	—
21 Sc	332.17 Dr.	329.28 Dr.	325.54 D.–S.	—	—
22 Ti	366.91 Dr. 366.94 F.	364.41 Dr.F. 364.32 F.	362.32 H. 361.95 F.	—	—
23 V	403.62 Dr. 403.63 F. 403.80 B. 403.34 403.95(V_2O_4) B.	400.98 D. 400.84 F.	398.75 H. 398.32 F.	—	394.0 B.
24 Cr	441.99 Fr. 442.13 B. 441.82 442.13(Cr_2O_3) B.	439.59 W. (Cr_2O_3)	436.91 D.–S.	—	431.5 B.
25 Mn	482.46 Dr. 482.06 483.23 B. 483.25(MnO) B. 482.97(MnS) B.	—	476.97 E.	—	Fe$K\alpha$ B.

Table I *Continued*

26 Fe	524.59 Dr. 524.41 B. 524.45 K.	522.32 K.	518.81 E.	—	512.0 B.
27 Co	568.34 B. 568.58 K.	565.97 K.	562.47 E.	—	555.0 B.
28 Ni	614.41 K.	611.56 K.	607.88 D.–S. E.	—	599.8 B.
29 Cu	—	659.32 K.	—	—	647.5 B.
30 Zn	710.87 B.	709.27 K.	—	—	696.3 B.
31 Ga	762.18 B.	—	—	—	746.3 B.
32 Ge	815.54 B.	—	—	—	803.8 B.
33 As	870.70 B.	—	—	—	—
34 Se	927.70 B.	—	—	—	—
35 Br	986.66 B.	—	—	—	—
37 Rb	1110.8 B.	—	—	—	—
38 Sr	1175.4 B.	—	—	—	—
39 Y	1242.9 B.	—	—	—	—

Historical

To account for the origin of the non-diagram lines of the K group, the following explanations have been proposed by various investigators.

(1) N. Seljakow and A. Krasnikow[1] suggested that the $K\beta'$ line is a diagram line and that the combination of the lines $K\beta_1$ and $K\beta'$ is a "relativity doublet". But its $\Delta\lambda$ does not coincide with the value calculated from the frequency difference of the M_{II} and M_{III} levels.

(2) G. Coster and J. M. Druyvesteyn[2] ascribed the origin of the $K\beta'$ line to the influence of the incomplete $M_{IV,V}$ shells on the $M_{II,III}$ levels, so this line is a component of $K\beta_1$. This view is opposed by G. Ortner[3].

(3) G. Ortner[3] assumed new M′ levels in the iron group and

1. N. Seljakow and A. Krasnikow, ZS. f. Phys. **33**, 601 (1925).
2. G. Coster and J. M. Druyvesteyn, ZS. f. Phys. **40**, 765 (1927).
3. G. Ortner, Wien. Sitzungsber. (IIa), **135**, 71 (1925); **136**, 369 (1927).

explained that the β' lines are the transitions from the M′ level to the K level.

(4) M. J. Druyvesteyn[1] has numerically confirmed that the lines $K\beta''$ and $K\beta'''$ are due to the electron transition from the M shell to the K shell of the atom singly-ionized at an M or L shell respectively.

(5) H. Beuthe[2] proposed that when (say) K- and L_{III} shells are ionized simultaneously by a swiftly moving cathode-ray electron, the M_V electron jumps to the ionized L_{III} shells and further jumps to the ionized K shell, and as a result the lines $K\beta\gamma$ and $K\beta\eta$ are emitted. Thus he calculated their wave-lengths as follows:

$$\nu\beta\gamma(Z)=\begin{cases}\nu\, K\alpha_1(Z)+\nu\, L\alpha_1(Z)\\ \nu\, K\alpha_1(Z)+\nu\, L\alpha_2(Z)\\ \nu\, K\alpha_2(Z)+\nu\, L\beta_1(Z)\end{cases}\qquad \nu\,\beta\eta(Z)=\begin{cases}\nu\, K\alpha_1(Z)+\nu\, Ll(Z)\\ \nu\, K\alpha_2(Z)+\nu\, L\eta(Z)\end{cases}$$

But if this idea is adopted, there are rather large discrepancies between the observed and the experimental values especially in the case of the line $K\beta\eta$.

(6) G. B. Deodhar[3] suggested that the $K\beta'$ line probably arises from the double jump $M_I \rightarrow L_{III}$ and $L_{III} \rightarrow K$, and calculated their wave-lengths, but the discrepancies seem to be rather large.

Theoretical

To establish a scheme for the non-diagram lines, the present author assumed two-electron jumps in a doubly-ionized atom obeying the Heisenberg selection rule[4] and arrived at a result which seems to account for the origin of the emission of these lines.

(I) *Doubly-ionized atom*

The possible modes of generation of a doubly-ionized atom are these: ionization by (i) a high-speed electron, (ii) X-rays, and (iii) *Auger* effect. In the elements here concerned the *Auger* effect is remarkably efficient in producing a multiply-ionized atom.

(II) *Two-electron jumps*

By two-electron jumps, the doubly-ionized atom changes into another doubly-ionized state. The difference of energy will be emitted as a

---

1. M. J. Druyvesteyn, ZS. f. Phys. **43**, 707 (1927).
2. H. Beuthe, *loc. cit.*
3. G. B. Deodhar, Roy. Soc., Proc. (A) **131**, 476 (1931).
4. M. Sawada, Mem. Coll. Sci. Kyoto Imp. Univ. (A) **14**, 248 (1931).

single quantum. Or more clearly to picture the process, it may be considered that, for example, by the transition of an electron of an outer orbit, the transition of an inner electron is *induced* and as the result of this process the atom emits a single quantum. Here it is assumed that this gives rise to a non-diagram line.

The non-diagram lines are known from element Y(39) to Na(11) for the $K\beta$ group. The energy levels there concerned are the electrons from the K, L_{I},....., and $N_{\text{II,III}}$ shells, although some of them disappear as we pass to light elements. Hence many doubly-ionized states can be imagined, and if we pick out two of them at random, a very great number of combinations may result. Here we need a selection rule.

(III) *Selection rules for two-electron transitions*

In optical spectroscopy it is known that in the arc spectrum of a calcium-like atom new series are found which H. N. Russel and F. A. Saunders[1] attribute to the simultaneous jumping of two electrons. In this case it has been proved theoretically by Heisenberg[2] that l_i for one of them must change by ± 1, and for the other by 0 or ± 2. This leads to the more general Russell-Laporte rule, and the quantum mechanical proof of it has been given by E. Wigner[3] and H. Weyl.[4] But the observed combinations are almost without exception included under the Heisenberg rule. Recently S. Goudsmit and I. Gropper[5] proved that when two electrons jump, one can change only its n, and the other changes its l by $+1$ or -1, and its n by an arbitrary amount, taking the first term of the series expansion for $1/r_{12}$ (where r_{12} is the distance between two electrons) in the electrostatic interaction. From their paper[5], it can be understood, after a little consideration, that this last rule is true irrespective of the type of $\{LS\}$ or $\{jj\}$ coupling. At any rate, it is assumed here that these rules are valid in the region of X-rays of light elements.

(IV) *The computation of the wave-lengths or* $\frac{\nu}{R}$*-values of the lines to be emitted by two-electron transitions*

---

1. H. N. Russell and F. A. Saunders, Astrophys. Journ. **61**, 38 (1925).
2. W. Heisenberg, ZS. f. Phys. **32**, 841 (1925).
3. E. Wigner, ZS. f. Phys. **43**, 624 (1927); **45**, 601 (1927).
4. H. Weyl, „Gruppentheorie und Quantenmechanik" 181 (1928).
5. S. Goudsmit and I. Gropper, Phys. Rev. **38**, 225 (1931).

For example take the combination of (LN) and (KM), then the outer electron of an atom of the atomic number Z moves the field of an atom of the next higher element, $Z+1$. So the emitted frequency during the reorganization of the atom is given by $\{M(Z+1)-N(Z+1)\}$. At the moment when the jumping of the inner electron occurs, an outer electron is absent, so the frequency emitted is not precisely given by $\{K(Z)-L(Z)\}$ although the correction will be of fairly small value. So here, as the $\frac{\nu}{R}$-values of the emitted frequency of a single quantum,

$$\{M(Z+1)-N(Z+1)\}+\{K(Z)-L(Z)\} \quad \text{.....(1)}$$

was chosen. This value of course must be equal to the energy change of the atom as a whole, namely,

$$\begin{aligned} KM(Z)-LN(Z) &= \{K(Z)+M(Z+1)\}-\{L(Z)+N(Z+1)\} \\ &= \{M(Z+1)-N(Z+1)\}+\{K(Z)-L(Z)\} \\ &\text{.....(2)} \end{aligned}$$

The term values are taken from various authors'[1] experimental and calculated values.

The various combination obeying the above selection rules were examined and finally the following combinations were found in best agreement with the experimental values and are collected in Table II.

In Fig. 1 the difference between the $\frac{\nu}{R}$-values of the $K\beta$ non-diagram lines and the diagram line $K\beta_1$, and the calculated values, is plotted against the atomic number.

The coincidence is rather good if we take into consideration the fairly rough values of the L_1 and M_1 levels which are computed with the irregular doublet law. So as to the transitions $KL_{II,III}-L_IM_I$ and $KM_{II,III}-M_IM_{IV,V}$, several computations were tried, various data given by different authors being used. These values are also plotted in Fig. I. The estimation of the line $\beta\eta$ is especially difficult owing to the lack of knowledge of the exact values of the L_I and M_I levels.

The $K\beta'$ lines have not yet been observed beyond the element copper, so that the discrepancies between the values of $KL_{II,III}-L_IM_{IV,V}$ and $K\beta_1$, may be due to the uncertainty as to the values of the $L_{II,III}$ levels.

---

1. R. Thoraeus, Phil. Mag. **1**, 312 (1926); **2**, 1007 (1926).
   G. Kellström, ZS. f. Phys. **58**, 511 (1929).
   C. E. Howe, Phys. Rev. **35**, 717 (1930).
   B. C. Mukerjee and B. B. Ray, ZS. f. Phys. **57**, 345 (1929).

If we take the values of the L_{II} and L_{III} levels separately, it can be readily shown that the value of $KL_{II,III} - L_I M_{IV,V}$ nearly coincides with that of $K\beta_1$. That is to say, the separation of β_1 and β' is small in these regions.

Thus we can ascribe the origin of the non-diagram lines of the $K\beta$ group to the following transition :—

Fig. 1

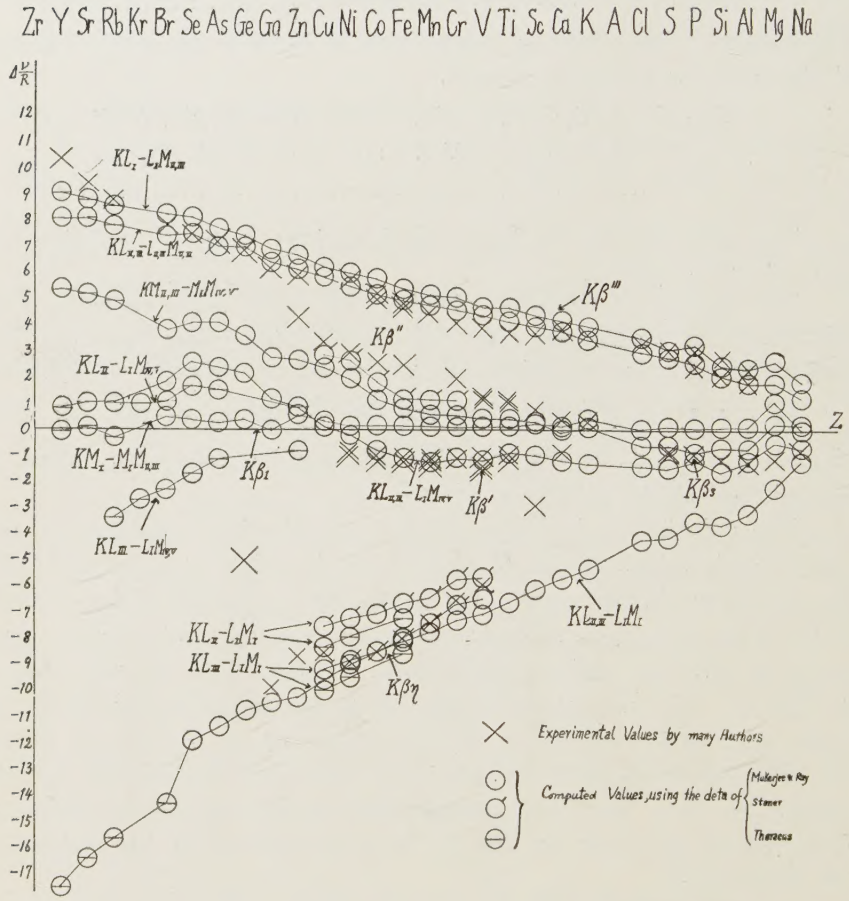

Table II

The calculated $\frac{\nu}{R}$-values of the lines expected from two-electron transitions.

Element	KL_{I}– $L_{I}M_{II,III}$	$KL_{II,III}$– $L_{II,III}M_{II,III}$	$KM_{II,III}$– $M_{I}M_{IV,V}$	KM_{I}– $M_{I}M_{II,III}$	$KL_{II,III}$– $L_{I}M_{I}$	$KL_{II,III}$– $L_{I}M_{IV,V}$
11 Na	80.515	79.914	78.838	78.647	77.437	77.998
12 Mg	98.188	97.570	95.829	96.665	93.401	95.117
13 Al	117.072	116.560	114.084	114.929	111.604	113.649
14 Si	137.665	137.220	134.545	135.326	131.636	133.649
15 P	160.616	159.960	156.609	157.399	153.942	156.252
16 S	184.509	184.240	180.890	181.627	177.419	180.076
17 Cl	210.873	210.321	206.712	207.420	203.171	205.977
18 A	240.711	240.140	236.294	236.972	232.377	235.335
19 K	268.292	267.810	264.452	264.812	259.114	263.114
20 Ca	299.662	299.220	295.490	295.664	289.888	294.38
21 Sc	332.970	332.450	328.850	328.804	322.482	327.58
22 Ti	367.890	367.300	363.672	363.336	356.656	362.32
23 V	404.384	404.060	400.176	399.839	392.707	398.610
24 Cr	443.062	442.550	438.527	438.090	430.773	436.976
25 Mn	483.187	482.760	478.657	478.226	470.305	476.834
26 Fe	525.207	524.790	520.631	519.959	511.779	518.807
27 Co	569.139	568.530	564.532	563.600	554.912	562.680
28 Ni	614.681	614.140	610.628	608.849	599.780	608.561
29 Cu	662.085	661.610	658.219	656.259	646.360	656.020
30 Zn	711.598	711.067	707.683	705.549	694.783	705.735
31 Ga	762.847	762.340	758.858	755.962	745.580	757.184
32 Ge	816.159	815.680	812.436	809.157	798.026	810.787
33 As	871.218	870.580	867.629	863.845	852.212	865.948
34 Se	928.261	927.720	924.334	920.619	908.335	922.760

1	KL_{I}	– $L_{I}M_{II,III}$	$K\beta'''$	11	KM_{I}	– $M_{I}N_{II,III}$	
2	$KL_{II,III}$	– $L_{I}M_{IV,V}$	$K\beta'$	12	$KM_{II,III}$	– $M_{I}N_{I}$	
3	$KL_{II,III}$	– $L_{I}M_{I}$	$K\beta\eta$	13	$KM_{IV,V}$	– N_{I}^{2}	
4	$KL_{II,III}$	– $L_{II,III}M_{II,III}$	$K\beta'''$	14	$KM_{IV,V}$	– $N_{I}N_{II,III}$	
5	$KM_{II,III}$	– $M_{I}M_{IV,V}$	$K\beta''$	15	$KM_{II,III}$	– $M_{II,III}N_{II,III}$	*not yet detected*
6	KM_{I}	– $M_{I}M_{II,III}$	$K\beta''$	16	$KM_{IV,V}$	– $M_{II,III}N_{I}$	
7	$KM_{II,III}$	– $M_{II,III}^{2}$	$K\beta''$	17	$KM_{IV,V}$	– $M_{IV,V}N_{II,III}$	
8	KL_{I}	– $L_{I}N_{II,III}$			. . . . .		
9	$KL_{II,III}$	– $L_{II,III}N_{II,III}$	*not yet detected*		. . . . .		
10	$KN_{II,III}$	– $N_{II,III}^{2}$					

(V) *Intensity or transition probability*

(a) By examining the results given above, we come to the following experimental rules as to the transition probability :—

(i) The interaction of the end orbit of the outer electron and the initial orbit of the inner electron is large, the transition probability is also large and the intensity of the emitted line is strong. For example, the combinations $KM_{II,III}-L_IN_I$, $KM_I-L_IM_{II,III}$ and $KM_I-L_{II,III}N_I$ are very weak and cannot be observed experimentally, and $KM_I-M_IM_{II,III}$ or $KL_{II,III}-L_IM_{IV,V}$ is fairly strong and can be observed in the spectrogram.

(ii) It is expected that the combination in which one electron is excited and another emits the energy cannot be found.

(iii) The combination in which the end orbit of the outer electron is on a lower energy level than the initial orbit of the inner electron cannot be found.

(b) It is expected that combination (10)–(17) will appear, but it is estimated that they will appear at the short wave-length side of the K absorption edge with few exceptions, so there is present an experimental difficulty due to the absorption of the radiation by the anticathode itself, as is also the case with $K\beta'''$.

(c) Now it is of interest to test the transition probability quantitatively. The group of transitions involving $K\rightarrow L_I$ is related to the emission lines of the L series and their intensity can be estimated, putting aside the question of coupling, as follows :

Non-diagram line	Origin	Related lines in the L series	Relative[1] intensity
$K\beta'''$	$(M_{II,III}\rightarrow L_I)+(L_I\rightarrow K)$	$L\beta_3+\beta_4$	0.08
not yet detected	$(N_{II,III}\rightarrow L_I)+(L_I\rightarrow K)$	$\gamma_3+\gamma_2$	0.02
$K\beta'$	$(M_{IV,V}\rightarrow L_{II,III})+(L_I\rightarrow K)$	$\alpha_1+\alpha_2+\beta_1$	1.00
$K\beta\eta$	$(M_I\rightarrow L_{II,III})+(L_I\rightarrow K)$	$l+\eta$	0.03
not yet detected	$(N_I\rightarrow L_{II,III})+(L_I\rightarrow K)$	$\gamma_5+\gamma_8$	0.003

This order of intensity is correct if we consider the coupling strength of two electrons there related.

(VI) *Term multiplicities*

Assuming pure $\{LS\}$ coupling, the following term multiplicities can be expected as the intense ones.

1. Allison & Armstrong, Phys. Rev. **26**, 714 (1925). These values are of W (74).

For example:

$K\beta\eta$	$^1S - {}^1P$,	$^3S - {}^3P$
$K\beta'(K\beta_3)$	$^3D - {}^3P$,	$^1D - {}^1P$
$K\beta'''(K\beta\gamma)$	$\begin{cases} {}^1P - {}^1S \\ {}^3P - {}^3S \end{cases}$	$\begin{cases} {}^1P - {}^1P \\ {}^1S - {}^1P \\ {}^3D - {}^3P \\ {}^3P - {}^3P \\ {}^3S - {}^3P \end{cases}$
$K\beta''$	$\begin{cases} {}^3D - {}^3P \\ {}^1D - {}^1P \end{cases}$	

In the case of satellites of $K\alpha$ the multiplets can be separated but in the case of $K\beta$ they cannot be separated but give only diffuse lines.

But it is reported that in the case of the line $K\beta'$ the breadth is greater for the lower elements and that it has been found to be two unresolved doublet-lines[1]. They are probably the lines $^3D - {}^3P$ and $^1D - {}^1P$, in pure $\{LS\}$ coupling, or due to the difference between L_{II} and L_{III} in pure $\{jj\}$ coupling. It is well known that the β''' line is also resolved in two components, especially in lower elements.

This is probably the transition of the type $KL_I - L_I M_{II,III}$, $KL_{II,III} - L_{II,III} M_{II,III}$ or some other included in the transitions (10)-(17) given in section (IV).

(VII) *The effect of chemical combination*

(i) *The $K\beta'''$ line* (*The $K\beta\gamma$ line*) Mn (25) – Ti (22)

H. Beuthe[2] examined the effect of chemical combination of some elements: Mn (25), Cr (24), and V (23). In every case one line appears or disappears and the other remains in sensibly the same place not influenced by the chemical valency. The line which appears or disappears is probably the line due to a valency electron cooperating in the two-electron transitions.

(ii) *The $K\beta''$ line* K (19), Ca (20)

This line is very weak and difficult to obtain. In potassium this $K\beta''$ line is probably due to the transitions $KM_I - M_I M_{II,III}$, so it will not be chemically influenced. This has been experimentally verified by O. Lundquist[3].

The $K\beta''$ line of calcium is probably of the same origin. In the elements beyond calcium, the line due to these transitions will be

1. V. Dolejšek & H. Fičláková, Nature, **123**, 412 (1929).
2. H. Beuthe, *loc. cit.*
3. O. Lundquist, ZS. f. Phys. **33**, 901 (1925).

superposed on the $K\beta_1$ line, and not separated as shown in Fig. 1.

(iii) *The $K\beta'$ Line* Ni (28)–K (19)

This line is greatly affected by chemical combination, as has been reported by many authors, especially G. Ortner[1].

This fact is clearly explained by the cooperation of an $M_{IV,V}$ electron in this transition. In an element where no electron exists in the $M_{IV,V}$ level, the $K\beta'$ line will be completely missing, and even if the β' line exists it will be very weak.

Actually, in potassium, this $K\beta'$ line is completely missing, and in calcium, it is very faint and hardly measurable.

(iv) *The $K\beta_3$ line* Cl (17)–Na (11)

The non-diagram line $K\beta_3$ is to be looked upon as the continuation of $K\beta'$ in the region Ni—Ca, as has been suggested by E. Hjalmar[2] and G. B. Deodhar[3].

According to my view, this speculation seems to be supported by the following experimental facts.

(1) In the chemical compounds of P (15), the β_2 line appears with the β_X line[4].

(2) In the chemical compounds of S (16), the β_3 line appears when β_X is stronger than β_1, the exception being some compounds where β_3 is very weak. But these compounds are expected to be unstable at the anticathode under the cathodic bombardment, and consequently it is not strange that the β_1 line is stronger than β_X.

On the whole the β_3 line is strong in the sulphate compounds.

(3 The β_3 line of pure sulphur listed by Hjalmar is suppressed by Deodhar[5].

(4) In Al (13), Mg (12), Na (11), the β_3 line was stronger in the case of the oxide than the pure metal.

---

1. G. Ortner, Wien. Sitzungsber. (**IIa**), **135**, 71 (1925); **136**, 369 (1927).
2. E. Hjalmar, *loc. cit.*
3. G. B. Deodhar, Roy. Soc. Proc. **A 131**, 476 (1931).
4. *Note on the origin of the* β_X *line.* It is well known that the cathode-ray bombardment and the consequent heating effects may cause a transformation of the substance placed on the anticathode. Therefore, the lines β_1 and β_X are the diagram lines due to the transition $M_{II,III} \rightarrow K$ in the destroyed element and compounds. From many experimental facts found by various authors, it seems to be verified that in the elements from Cl (18) to P (15), the long wave-length one is due to free element and the short wave-length one is due to the chemical compound, and from Si (14) to Na (11) the reverse is the case. The cause of this peculiar fact is probably intimately related to the fact that the elements from Cl (17) to P (15) are electronegative, and those from Al (13) to Na (11) are electropositive.
5. G. B. Deodhar, *loc. cit.*

From the above-cited evidence, it can be accepted that the chemical compound gives the β_3 line strongly.

In the present scheme, the origin of the β_3 line is the transition $KL_{II,III} - L_I M_{IV,V}$.

The objection to this view is that the existence of the $M_{IV,V}$ electron in the lower elements has been questioned. Dealing with this point, recently F. London[1] showed that in the homopolar compound the distributions of the electrons are as follows :—

Element	Homopolar valency	No. of electrons		
		M_I	$M_{II,III}$	$M_{IV,V}$
P (15)	1	2	3	
	3	2	3	
	5	1	3	1
S (16)	0	2	4	
	2	2	4	
	4	2	3	1
	6	1	3	2
Cl (17)	1	2	5	
	3	2	4	1
	5	2	3	2
	7	1	3	3

In heteropolar compounds like MgO and Al_2O_3, all of the valency electrons cannot be considered as they are completely transferred to the oxygen atom[2]. At least one electron will exist in the $M_{IV,V}$ levels or the $M_{II,III}$ levels of Mg or Al atoms.

So the line β_1 ($M_{II,III} \rightarrow K$) should not be taken as a semioptical one.[3]

And also there is a chance that the β_3 line will appear.

Thus it can be concluded that some elements—in chemical combination and in the solid state, the $M_{IV,V}$ levels are occupied by the valency electrons—will give rise to strong β_3 lines.

(v) *The $K\beta_4$ lines.*

In very stable compounds on the anticathode, such as strontium

1. F. London, ZS. f. Phys. **46**, 455 (1928); R. Swinne, Chemiker-Kalender **50, III,** 63 (1929).

2. Wyckoff, The Structure of Crystals, 272 (1924).

3. In the case of the halide of Na, the ionization is complete and really the β_1 line is very difficult to obtain compared with that of Na_2O.

sulphide, barium sulphide, cadmium sulphide, the β_4 line was found. This β_4 line together with the β_4 line of P and Si is probably the continuation of the non-diagram line $\beta\eta$ in the region Ge—V, detected by Beuthe[1] and in the case of Ti by the author[2].

Remarks

(1) The lines $K\beta\eta$ of Ge and $K\beta'$ of Sc deviate from the $\frac{\nu}{R}$-curves of $K\beta\eta$ and $K\beta'$.

But these are fitted into the transition of the type $KM_{\mathrm{I}}-M_{\mathrm{I}}^2$, although this is forbidden by the present scheme.

(2) *The origin of non-diagram lines of the Kα group*

If the rules mentioned in (V) (a) (i), (ii) and (iii) are valid, the origin of the $K\alpha$ satellites may be expected to be the transitions $KL_{\mathrm{I}}-L_{\mathrm{I}}L_{\mathrm{II,III}}$ and $KL_{\mathrm{II,III}}-L_{\mathrm{II,III}}^2$. This scheme agrees with the recently published result of R. M. Langer[3].

In conclusion the author wishes to express his hearty thanks to Prof. M. Ishino for his kind guidance and the interest he has taken in this research, and also to Prof. M. Kimura, Dr. Y. Nishina and Mr. S. Kawata for much valuable advice during this work.

1. Beuthe, *loc. cit.*
2. M. Sawada, *loc. cit.*
3. R. M. Langer, Phys. Rev. **37**, 457 (1931).

Biochemical Study on the Autumn Fall of the Leaf

By

Shigeru Komatsu and Shinsaku Ozawa

(Received January 8, 1932)

Numerous investigations have been reported by physiologists and chemists on the autumn fall of the leaf, a remarkable feature of the plants growing in countries with alternating wet and dry, or warm and cold seasons[1]. Among these, the research work by S. Kaeriyama[2], dealing with the Ginko tree (*Ginko biloba, L.*) and the cherry tree (*Prunus donarium, Sieb.*), is of great interest; estimating the reducing sugars and starch and dextrin in the fallen leaves and branches at the same time, and comparing the leaves and stems gathered in May and in December, with respect to the content of crude protein, ether extract, crude fibre, total ash, and especially of the composition of the ash, he came to the conclusion that the object of the autumnal shedding of the leaves is not thrown away substances useless for the life of the plant, though the yellow coloured leaves, as other investigators have reported[3], contain in their ash constituents more Na, Ca and S but less K, N and P than the green ones. However, he said nothing with regard to the hypothesis put forward by Sachs in his study of plant physiology, but opposed by Wehmer[4], that substances useful for the life of the plant migrate from the leaves to the stems before winter comes.

Other plant biologists have supposed that when the leaves are exhausted of the mineral and organic substances required for leaf-

1. Michel-Durand: Variation des Substances hydrocarbonees dans les feuilles. 1917.
2. J. Chem. Soc., Tokyo, **32**, 964 (1902).
3. E. Stahl: Zur Biologie des Chlorophylls, s. 139 (1909).
4. Ber. D. Bot. Gess., **10**, 152 (1892).

activity, or when winter comes to reduce the risk of desiccation of the plant, the evaporation of moisture from the leaves is prevented by the forming of a layer of cork near the base of the leaf stalk, and the leaves are then broken off by the atmospheric agencies or drop by their own weight to the ground.

The object of this experiment was to find out what chemical changes in the leaf constituents take place in the life history of the leaves, and if possible to find the physiological meaning of the autumn leaf-fall. The leaves of the ginko tree were therefore examined, since this tree is very common in Japan and moreover, the leaves change their colour quite uniformly and then almost all the leaves fall simultaneously.

The samples of the leaf used for the experiment, except the last dated one, shown in the following table, were plucked once a month at 10 o'clock on fine mornings, from the southern branches—about 3–4 meters above the ground—of the two ginko trees growing side by side in the garden of the Buddhist temple, Hyakumanben Tion-di, located about 100 meters from the laboratory. The last sample was gathered at 8 o'clock on Nov. 19th from the leaves fallen on the ground under the trees which had been cleared of fallen leaves at 5 o'clock the previous evening; the fallen-leaves, among which there were no green-tinged ones, were quite uniform in maturity.

In these samples, the hydrogen-ion concentration of the cell-sap and the content of moisture, ash, ether-soluble matter, nitrogenous matter, chlorophyll, carbohydrates and crude fibre were determined by the following methods :—

1. pH-value: the cell-sap of the leaves was prepared by crushing them in a mortar and its pH-value was determined by the electrometric method, since the concentration of leaf-sap, in the case of leaves poor in juice-content, varies, as observed by Y. Yamaguchi[1], according to the method of preparation, and crushing the leaves in a mortar gives good results for the present purpose. In the determination of the pH-value, the experiment was carried out on the day on which the sample for analysis was collected, and again on the day after, and the mean value of the two determinations was taken.
2. Moisture: about 5 gms. of the fresh leaves were dried to a

1. J. Chem. Soc., Tokyo, **41**, 729; and also refer to Atkins, "Some Recent Researches in Plant Physiology", p. 86 (1916), and H. H. Dixon, "Transpiration and the Ascent of Sap in Plants". p. 175 (1914).

constant weight in an air bath heated at 103–105°, and the loss of weight was designated moisture-content.

3. Ash-content: the sample, dried as above, was incinerated in the usual way.

4. Ether-soluble matter: the sample was finely pulverised after being dried in a vacuum sulphuric acid desiccator and treated with ether to extract fatty compounds.

5. Nitrogen-content: the total nitrogen in the fresh leaves was determined by Kjeldahl's method and also the nitrogen-content in both water and alcohol extracts was estimated.

6. Chlorophyll-content: the leaves, dried in a vacuum desiccator, were treated with acetone to extract chlorophyll and its content was calculated by multiplying the nitrogen-content in the extract by 150.

7. Carbohydrates: 50 gms. of the fresh leaves were dipped in alcohol, containing calcium carbonate to neutralize organic acids in the tissues, to dry the leaves, filtered and then minced finely, and treated successively with 90 % alcohol at a temperature of about 60°, with hot water, with a hot 1 % hydrochloric acid and finally with a hot 1.25 % caustic soda solution to extract simple sugars, disaccharides, starch-like substances and pentosan respectively.

The two alcohol solutions were put together and the solvent was distilled off under reduced pressure. The residue was then dissolved in water and the solution clarified with neutral lead acetate solution and sulphuretted hydrogen, and the sugar content in the clarified solution was estimated by determining the reducing power before and after hydrolysis with 2.5 % hydrochloric acid.

The hot water extract was clarified as before with lead acetate solution and sulphuretted hydrogen, and the content of maltose in the solution was estimated by its reducing power after being hydrolysed with 2.5 % HCl.

The starch-content in the leaves was estimated with the 1 % HCl extract by determining the reducing power of the solution after it had been clarified in the usual manner and neutralized with caustic soda.

8. The cellulose-content: the residue of the alkaline extract was washed with water and dried, and the difference between this and the ash-content was designated crude fibre.

In the determination of carbohydrates, the reducing power of the solution was determined by the Munson-Walker method[1] and the results were expressed as d-glucose.

1. J. Am. Chem. Soc., **28**, 663 (1906).

The experimental results are shown in the following table. In the table the content of ether-sol. matter, crude fibre, and other constituents are expressed on an ash-free and dry basis.

Date	Appearance of leaf	pH	Moisture %	Ash %	Ether extract %	Chlorophyll %
June 18	green	3.7	72.74	1.37	—	1.51
Aug. 8	green	3.1	73.32	1.65	12.55	1.56
Sept. 8	green	3.1	74.57	1.84	14.79	1.23
Oct. 8	gr., slightly yellow	3.6	75.21	1.89	14.28	1.14
Nov. 7	greenish yellow	3.5	76.99	1.76	16.68	0.99
Nov. 19	almost pure yellow	3.2	73.51	2.48	15.12	0.46
Nov. 21	yellow slightly brown	3.6	71.88	2.14	17.55	0.50

Date	Total N	Soluble N		Insoluble N	Soluble N (% in Total N)		
		alc. extract	water extract		alc. extract	water extract	Total
June 18	2.70	0.31	0.15	2.24	11.4	5.7	17.1
Aug. 8	2.45	0.39	0.20	1.86	16.0	8.2	24.2
Sept. 8	2.68	0.19	0.08	2.41	7.1	2.8	9.8
Oct. 8	2.22	0.17	0.09	1.96	7.7	4.1	11.8
Nov. 7	1.42	0.26	0.12	1.04	18.6	8.5	26.1
Nov. 19	0.99	0.23	0.12	0.64	23.4	12.1	35.5
Nov. 21	0.95	0.20	0.09	0.65	21.3	9.9	31.2

Date	Soluble carbohydrates		Starch	Total carbohydrates	Crude fibre
	reducing	non-reducing			
June 18	—	—	—	—	19.66
Aug. 8	1.44	9.87	2.76	14.07	27.37
Sept. 8	2.25	8.73	3.01	14.04	26.66
Oct. 8	2.77	9.33	2.40	14.50	28.60
Nov. 7	4.94	3.67	1.98	10.59	30.54
Nov. 19	2.25	3.70	2.75	8.70	34.44
Nov. 21	2.31	2.77	2.08	7.16	32.61

As may be seen from the experimental results, the pH-value of the press-juice was 3.7 on June 18th; this decreased gradually to 3.1 on September 8th and increased again to 3.6 in October, and the monthly variation of the pH-value is reciprocal with that of the total soluble nitrogenous substances.

The percentage of moisture increased gradually from 72.7 % on June 18th to the maximum value 77 % on Nov. 7th and then decreased suddenly to 73.5 % on Nov. 19th before the leaf-fall. The ash-content changes with age in the same way as the moisture content.

The content of reducing sugars increases gradually till the leaf begins to be coloured yellow and after this period the content decreases rapidly as yellow shade of the leaves increases.

Fig. 1

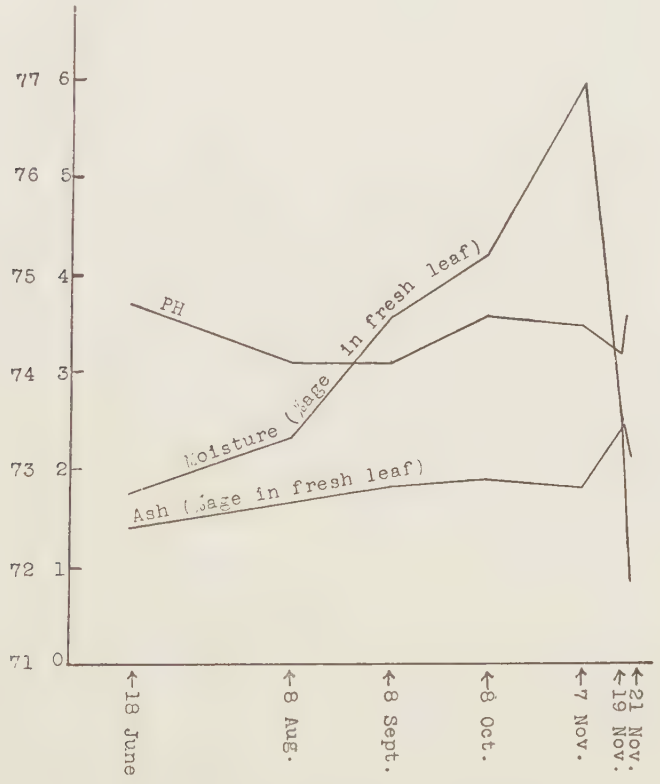

The content of sugar hydrolysible with 1 % HCl, mostly a starch-like substance, changes inversely with the simple sugars. The content of non-reducing soluble sugars remains almost constant till October and then decreases rapidly with progress of time. The content of total carbohydrates consequently remains constant till October and then decreases suddenly before winter comes, while the crude fibre increases with age.

The chlorophyll-nitrogen content shows a decrease through the life-history of leaf, but on the other hand the content of ether extract increases steadily.

Fig. 2

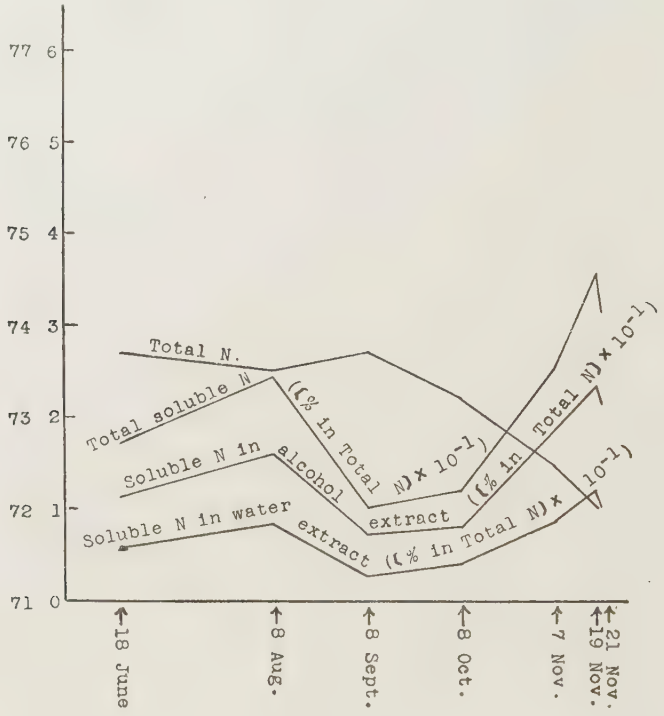

Discussion of the Results

The pH-value of the cell-sap shows a close relationship, in numerical value, with the content of the water-soluble nitrogenous matter; at the end of summer the cell-sap shows strong acidity and the water soluble nitrogen in the same season shows the minimum value and the insoluble N the maximum; but when autumn comes the acidity of the cell-sap decreases suddenly owing to an increase in the soluble nitrogenous matter. The seasonal variation of the nitrogenous matters, which are usually regarded as intimately connected with the activity of plant tissues, is noteworthy. The content of the total N decreases with time though that of the soluble N shows a minimum in autumn and a maximum at the end of summer and also the

beginning of winter, and we have put forward the hypothesis based on these facts that the decomposition of cytoplasmic material and the transition of the soluble nitrogenous matter formed by the decomposition of proteins from leaves to stems occurs when the leaves are mature. This hypothesis to explain the metabolism of nitrogenous substances in the leaves of higher plants is partly in agreement with the opinion of Chibnall, who investigated the diurnal variations in the protein nitrogen of Phaseolus vulgaris[1].

Fig. 3

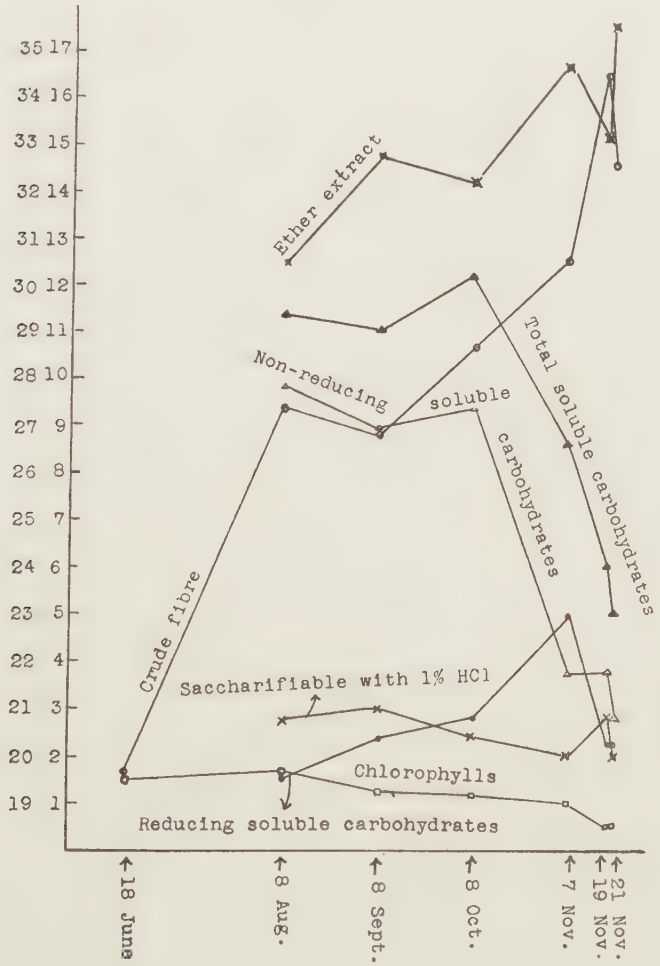

1. Chibnall: Bioch. Jour., **18**, 387 (1924).

The moisture content, as may be seen in the table and figure, increases continuously till the end of autumn and decreases suddenly when winter comes. This finding is opposed to the observation made in plant-leaves by Andre[1], and may be explained by assuming that the respiration of the leaf-cell will take place vigorously in autumn by reason of which water, one of the products of respiration, is stored in the cell-sap without evaporation to the surrounding air owing to the high degree of humidity of the atmosphere in that season, as may be seen from the atmospheric conditions of the year, observed in the Laboratory of Agricultural Technology of Kyoto, shown in the following table.

Date	Humidity at 10 a.m.	Max. humidity preceding it	Temperature at 10 a.m.	Lowest temp. early that morning	Max. temp. of the previous day
June 18	—	—	—	—	—
Aug. 8	75	95 at 5 a.m.	28.3°	21.7°	29.4°
Sept. 8	75	99 „ 6 „	29.4	24.4	31.7
Oct. 8	90	100 „ 8 „	22.8	15.0	26.7
Nov. 7	90	100 „ 9 „	10.6	1.1	15.0
Nov. 19	—	—	18.3	11.1	17.8
Nov. 21	—	—	—	—	15.6

The metabolic changes in the nitrogenous matter in the ginko leaves seem to occur, as we understand from Figs. I & II, in an opposite way to the seasonal variation of the carbohydrate content, but the latter changes in the same way as the water-content.

The fact that the reducing sugar-content changes in parallel with the water-content suggests that the water in the tissues plays an important part in the hydrolysis of polysaccharides, and indeed the content of starch-like substance shows a maximum at the end of summer and a minimum at the end of autumn.

Conversion of the non-reducing soluble sugars into crude-fibre in the tissues is supposed to occur, from the relation of their content in various seasons, and the polymerisation of the lower saccharide into the higher molecular one—cellulose—as we learned from the heat of formation of these substances, is accompanied by the absorption of heat. As a matter of fact, the formation of cellulose in the leaves occurs mostly in summer, which is to be expected from van't Hoff's

1. C. R., **148**, 1685 (1909).

law of mobile equilibrium. The accumulation of reducing sugars and of cellulose which occurs actually in the leaf before winter comes may be explained in the following way :—the hydrolysis of starch-like substances is the chief factor in the origin of reducing sugars and the formation of cellulose is due to polymerization of non-reducing soluble sugars. Such antagonistic chemical changes in the carbohydrates—hydrolysis and polymerization—were also noticed to occur in plants by Michel-Durand, but the polymerization of carbohydrates, in her case, was expressed as characteristic feature of plants which is observed from spring to the end of summer.

Such a difference between our results and those of European investigation in the water content of the leaves in autumn and also in the carbohydrate content between ours and Europian investigators' must be attributed to the difference in the environmental conditions of Japan and the West.

It seems that *one of the most important functions of the autumn leaf-fall is to enable the plant to get rid of inorganic materials—ash—so that the accumulation of the ash constituents is prevented from controlling the metabolic changes of the tissue materials and the plant is able to live a normal life in winter.*

But the fate of the plant ash in vegetation is a matter of speculation when we observe ever-green trees, the leaves of which remain attached to the tree till, after some years, one by one they fall from old age. This problem will be discussed again in the near future on an article from this laboratory.

April, 1926.

Laboratory of Organic- & Bio-Chemistry.

The Diffusion of Zinc in Copper and its Alloys[1]

By

Yoshito Yamauchi

(Received January 11, 1932)

Iron or steel coated with brass stands comparison with brass in the properties relating to its surface such as resistance against corrosion, while in mechanical properties it is superior owing to the iron or steel inside. Brass coating can be done by the following methods: 1. Electro-plating; 2. metal spraying; 3. the dip process, and 4. the method in which iron or steel is first coated with copper and then the latter is converted into brass by zinc diffusion brought about by heating it in contact with zinc vapour.

The diffusion of zinc in copper is an important problem to the author, who has studied the last two methods.

A number of investigations[2] have been carried out in connection with this problem, but all of them except that of Elam[3], who heated copper in contact with zinc vapour and examined the microstructure, were made with specimens in which these two metals came in contact with each other.

Dunn[4] studied the rate of diffusion in solid brass by measuring the loss of zinc observed on weighing after heating at different temperatures for different periods of time in vacuo. He found the relation between the amount of zinc lost and the composition of brass, as well as the temperature and the duration of heating, but his study is

1. This was read in part at the Meeting of the Chemical Society of Japan, April. 1930.

2. O. F. Hudson: Journ. Inst. Metals, **12**, 94 (1914); J. H. Andrew and R. Higgin: Ibid., **28**, 185 (1922); O. Bauer and E. Piwowarsky: Metal u. Erz, **20**, 416 (1923); S. L. Hoyt: Amer. Inst. Min. Met. Eng. Tech. Publ., No. 128 (1928); W. Kohler: Journ. Inst. Metals, **39**, 493 (1928) (Abstract).

3. C. F. Elam: The Inst. of Metals, Advanced Copy, No. 158 (1930).

4. J. S. Dunn: Journ. Chem. Soc., 2973 (1926).

restricted within the α range. The author therefore studied this problem in connection with his coating practice, as described below.

I. Experiments with Copper and Zinc

1. Specimen

Cast Copper:—Pure electrolytic copper was melted in a graphite crucible in a coke fired oven, molten sodium chloride being used as a cover, and cast in a preheated iron mould with a hole 12 mm. square in section and 170 mm. in length. Specimens of 5 mm. in thickness were prepared by cutting these bars.

Rolled Copper Plate:—Rectangular specimens, 14 mm. in width and 26 mm. in length, were prepared from rolled pure electrolytic copper plate of about 0.9 mm. thickness.

2. Experimental Procedure

After being weighed and its surface area measured, a cast copper specimen was placed on a support in the centre of a porcelain boat. Pure granular zinc was placed on both sides of this support so that it was not in contact with the specimen. Then the boat was placed in the centre of a glazed porcelain tube which was put into a nichrome furnace.

A slow current of purified dry hydrogen was first passed through the tube for 15—20 minutes in order to replace the air, whereupon the cork provided at the end of apparatus was closed so as to cut off the flow of hydrogen, but the whole apparatus was thus protected from air by hydrogen under pressure. Now it was heated to the desired temperature[1] and kept at that temperature, with variations within $\pm 3^{\circ}$C., for the desired period and then cooled. The specimen was then weighed. The amount of zinc[2] diffused in the copper per unit surface was calculated by dividing the total weight increase by the surface area of the specimen.

In the experiments with copper plate specimen, the porcelain boat, 13.8 mm. in width and 25.7 mm. in length and containing pure granular zinc at the bottom, was covered with the specimen.

---

1. It reaches 900°C. within 10 minutes.
2. This was checked by analysis in a few cases.

3. The Influence of Temperature

The experimental values obtained by keeping the specimen for half an hour at temperatures ranging from 400° to 650°C. are given in Tables I and II.

Table I

Cast Copper: Duration of Heating = 30 minutes

Temp. °C	$1/T \times 10^3$	Weight of Specimen in gms.	Surface Area of Specimen in sq. cms.	Weight-increase		$\log \Delta W$
				in gms.	in gms./sq. cm. ΔW	
405	1.4749	5.7634	4.87	0.0045	0.0009	$\bar{4}.9657$
434	1.4144	5.9904	4.75	0.0104	0.0022	$\bar{3}.3403$
450	1.3834	6.7194	5.09	0.0173	0.0034	$\bar{3}.5313$
457	1.3699	5.3337	4.67	0.0198	0.0042	$\bar{3}.6274$
478	1.3316	5.8217	4.60	0.0307	0.0067	$\bar{3}.8244$
501	1.292	5.9481	5.01	0.0599	0.0120	$\bar{2}.0776$
506	1.2837	6.8571	5.07	0.0623	0.0123	$\bar{2}.0895$
550	1.215	5.3627	4.73	0.1602	0.0339	$\bar{2}.5298$
554	1.2092	5.8396	4.94	0.1664	0.0337	$\bar{2}.5274$
590	1.1588	5.2748	4.29	0.2764	0.0644	$\bar{2}.8091$
601	1.1442	5.6571	4.87	0.3797	0.0780	$\bar{2}.8919$
602	1.1428	4.8060	4.37	0.3370	0.0771	$\bar{2}.8872$

Fig. 1

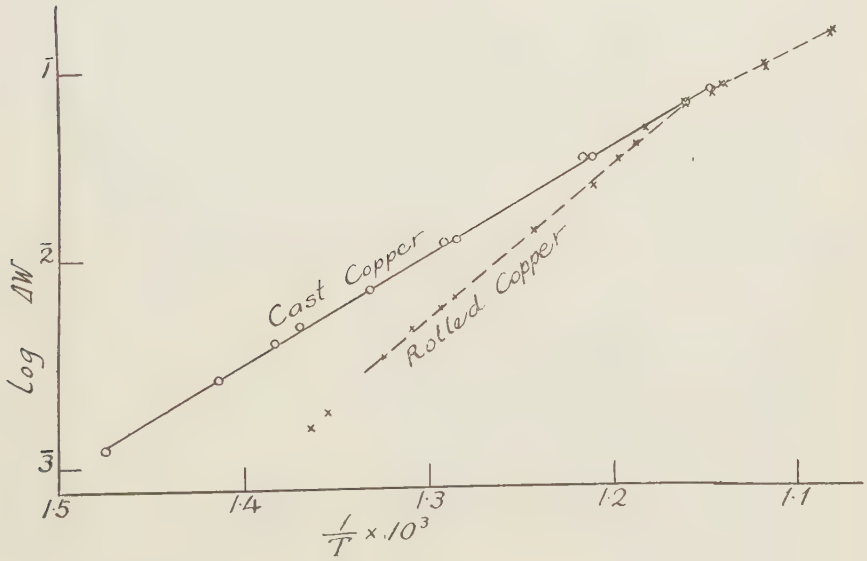

Table II

Rolled Copper: Duration of Heating=30 minutes

Temp. °C	$1/T\times10^3$	Weight of Specimen in gms.	Surface Area of Specimen in sq. cms.	Weight-increase		log ΔW
				in gms.	in gms./sq. cm. ΔW	
460	1.3643	2.9198	3.72	0.0044	0.0012	3.073
465	1.355	2.8308	3.66	0.0052	0.0014	3.1525
480	1.328	2.8248	3.64	0.0102	0.0028	3.4475
491	1.309	2.7575	3.50	0.0141	0.0040	3.605
500	1.2937	2.9234	3.74	0.0196	0.0052	3.7194
505	1.2854	2.8100	3.62	0.0217	0.0060	3.7778
532	1.2422	2.9094	3.76	0.0509	0.0135	$\bar{2}$.1315
554	1.2091	2.8898	3.70	0.0867	0.0234	$\bar{2}$.3698
563	1.1962	2.9204	3.76	0.1231	0.0328	$\bar{2}$.515
571	1.1862	2.9213	3.71	0.1458	0.0393	$\bar{2}$.5943
583	1.1683	2.8700	3.66	0.1776	0.0485	$\bar{2}$.686
590	1.1588	2.8372	3.68	0.2316	0.0629	$\bar{2}$.799
590	1.1588	2.8478	3.64	0.2346	0.0645	$\bar{2}$.8092
601	1.1442	2.8630	3.64	0.2668	0.0733	$\bar{2}$.865
605	1.1392	2.8892	3.67	0.3002	0.0818	$\bar{2}$.9127
607	1.1364	2.9284	3.67	0.3046	0.0830	$\bar{2}$.919
624	1.1148	2.8553	3.68	0.3939	0.1070	$\bar{1}$.0295
625	1.1136	2.9210	3.75	0.3784	0.1009	$\bar{1}$.0039
625	1.1136	2.9081	3.71	0.3799	0.1024	$\bar{1}$.0103
654	1.0788	2.9308	3.74	0.5703	0.1525	$\bar{1}$.1832
655	1.0776	2.8407	3.63	0.5901	0.1626	$\bar{1}$.211
655	1.0776	2.8431	3.70	0.6049	0.1635	$\bar{1}$.2135

In Fig. 1, the logarithm of the amount of zinc diffused into copper per unit area (log ΔW) is plotted against the reciprocal of the absolute temperature ($1/T$).

As straight lines are obtained for both cast copper and rolled copper, the relation between ΔW and T will be expressed by the following equation

$$\Delta W = A e^{-\frac{B}{T}}$$

where A and B are constant.

At low temperatures, the amount of zinc diffused per unit area gives lower values for rolled copper than for cast copper. As the temperature rises, however, the former gradually approaches the latter, with the removal of its deformation owing to the recrystallisation, so that both give the same value at about 600°C.

4. The Influence of Time

To study how the diffusion is related to time, the both cast and rolled specimens were heated in contact with zinc vapour at certain

Table III

Cast Copper

Temp. °C	Weight of Specimen in gms.	Surface Area. of Specimen in sq. cms.	Time in hrs.	Weight-increase	
				in gms.	in gms./sq. cm.
435	5.3640	4.34	0.5	0.0071	0.0016
	5.9904	4.75	0.5	0.0104	0.0022
	5.8050	4.60	1.0	0.0135	0.0029
	5.5650	4.53	1.5	0.0192	0.0042
	6.1595	4.75	2.0	0.0240	0.0051
	5.5413	4.56	2.5	0.0277	0.0061
	6.0257	4.70	3.0	0.0312	0.0066
478	5.8217	4.60	0.5	0.0307	0.0067
	5.7122	4.55	1.0	0.0455	0.0100
	5.6600	4.48	1.0	0.0455	0.0102
	6.0211	4.68	1.5	0.0630	0.0135
	6.4200	4.93	1.5	0.0691	0.0140
	5.7632	4.55	2.0	0.0716	0.0157
	6.3824	4.92	2.0	0.0846	0.0172
	5.3568	4.45	2.5	0.0880	0.0198
	5.4836	4.39	3.0	0.0989	0.0225

Table IV

Rolled Copper: Temperature = 550°C

Weight of Specimen in gms.	Surface Area of Specimen in sq. cms.	Time of Heating in hrs.	Weight-increase	
			in gms.	in gms./sq. cm.
2.8932	3.68	0.5	0.1120	0.0304
2.8753	3.70	1.0	0.2165	0.0585
2.8550	3.66	1.0	0.2124	0.0580
2.8957	3.65	1.5	0.2837	0.0777
2.8948	3.69	2.0	0.3552	0.0963
2.9141	3.72	2.0	0.3636	0.0977
2.8760	3.70	2.5	0.4254	0.1150
2.8790	3.68	2.5	0.4110	0.1117
2.8335	3.68	3.0	0.4597	0.1249

definite temperatures for 1/2—3 hours. The results are given in Tables III and IV and are plotted in Fig. 2 and Fig. 3.

Fig. 2

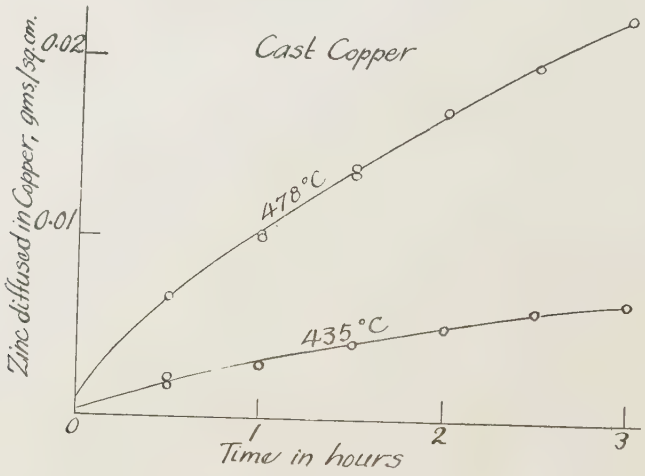

Fig. 3

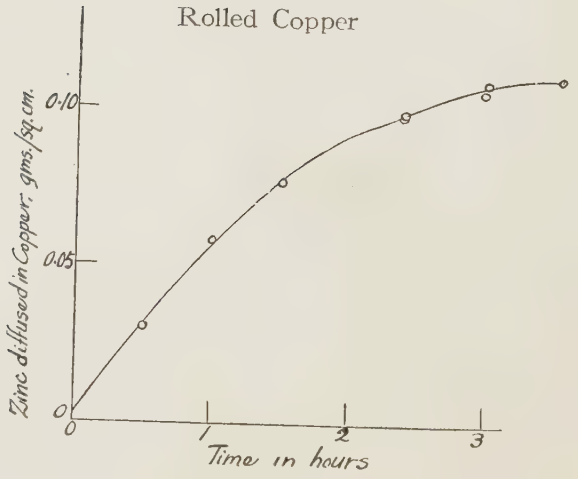

5. Appearance and Microstructure

Copper heated in contact with zinc vapour became coated with brass, and its colour turned light yellow or white according to the temperature and the time of heating : these changes were accompanied by expansion. The copper plate specimens, which were placed over

the boat, so that the diffusion occurred only from the surface facing the boat, bent upwards owing to the expansion of this surface. If the specimen was cubic in form, only its corners and their vicinity became white, these being the places where the penetration of zinc took place from the adjacent surfaces and was greatest in its amount, while the middle parts of the surfaces were yellow and there were very sharp lines of demarcation between the yellow and the white parts.

After the layer that looked yellow with the naked eye had been removed by grinding, the polished sections were examined under the microscope. Photo No. 1 shows the structure of a specimen heated three times for 30 minutes at 500°C, in which 0.0328 gm. of zinc was absorbed per unit surface, and No. 2 that of one heated for 30 minutes at 600°C with a gain of 0.0780 gm. per unit surface of the specimen. Both consist of homogeneous α solid solution in the outer layer, while in the inner area, the diffusion proceeds along grain boundaries, leaving in places a grain wholly converted into α brass.

II. Experiments with Brass

1. Specimen

For the preparation of the specimens, pure zinc and pure electrolytic copper were taken in the required proportions and melted in a graphite crucible in a coke fired oven under molten sodium chloride in order to avoid changes in composition by volatilisation of zinc and oxidation. After the melt had been thoroughly stirred, it was cast in a preheated iron mould with a hole 10 mm. in diameter and 150 mm. in length. These rods were then turned and cut.

The copper content was determined with their turnings by duplicate volumetric analysis.

2. Experimental Procedure

The weighed specimen, of which the surface area was measured, was heated in a hydrogen atmosphere, in the same manner as described in the experiments with copper and zinc.

3. The Influence of Composition

The amount of zinc lost per unit surface in half an hour at 850°C

was estimated with brasses[1] of various zinc contents, up to about 36%. The experimental data are given in Table V and are shown in Fig. 4 where the circles denote the actual amounts of zinc lost and the crosses the logarithms of these numbers.

Table V

Temperature=850°C.: Time=30 minutes

Copper Content in %	Weight of Specimen in gms.	Surface Area of Specimen in sq. cms.	Weight-decrease		log ΔW
			in gms.	in gms./sq. cm. ΔW	
94.4	4.0218	3.27	0.0022	0.0007	$\bar{4}$.8279
	3.8671	3.21	0.0023	0.0007	$\bar{4}$.8552
89.8	3.8256	3.18	0.0037	0.0012	$\bar{3}$.0658
	3.8516	3.22	0.0038	0.0012	$\bar{3}$.0719
84.6	3.8176	3.19	0.0076	0.0024	$\bar{3}$.3770
	3.8048	3.19	0.0076	0.0024	$\bar{3}$.3770
80.3	3.6458	3.13	0.0138	0.0044	$\bar{3}$.6443
	3.9350	3.29	0.0138	0.0042	$\bar{3}$.6272
75.5	3.6510	3.13	0.0260	0.0083	$\bar{3}$.9194
	3.6840	3.16	0.0265	0.0084	$\bar{3}$.9236
64.2	3.8910	3.32	0.1290	0.0389	$\bar{2}$.5895
	4.0079	3.37	0.1290	0.0383	$\bar{2}$.5830

Fig. 4

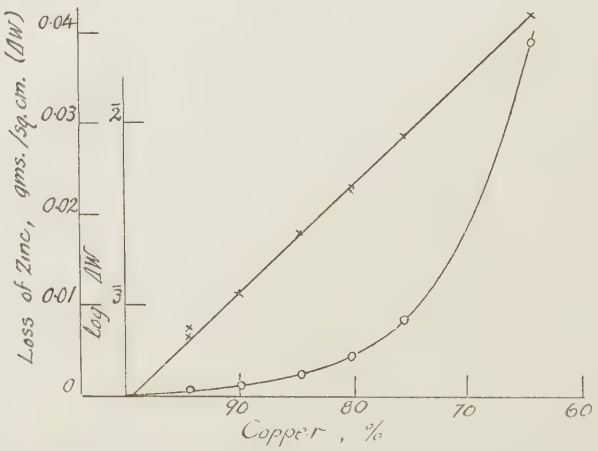

1. These specimens were prepared from alloys melted in a Tammann tube.

As is evident from these results, the amount of zinc lost (ΔW) varies exponentially with the zinc content (C) in the α range, establishing the following equation :—

$$\Delta W = ae^{bc}$$

where a and b are constants. Dunn's results[1] agree with this.

From the results obtained in experiments II–4, some of which were calculated by interpolation, the logarithms of the amounts of zinc lost from unit surface at 850° and 800°C. with brasses containing 70—50 % copper were plotted against their composition and are shown in Fig. 5.

Fig. 5

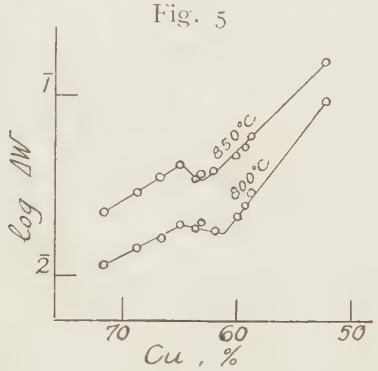

In the case of the brasses ranging over the α, $\alpha+\beta$, and β fields, however, they are not continuous straight lines but show breaks at those points corresponding to the composition near the boundary between different fields.

In connection with the above experiments, three specimens of different compositions put side by side were heated for 30 minutes at 670°C. with the results given in Table VI and Fig. 6.

Table VI

Copper Content in %	Weight of Specimen in gms.	Surface Area of Specimen in sq. cms.	Weight-change	
			in gms.	in gms./sq. cm.
89.97	4.3374	3.48	+0.0056	+0.0016
70.62	3.7115	3.22	−0.0027	−0.00084
61.34	3.9800	3.36	−0.0288	−0.0086

1. J. S. Dunn: loc. cit.

Fig. 6

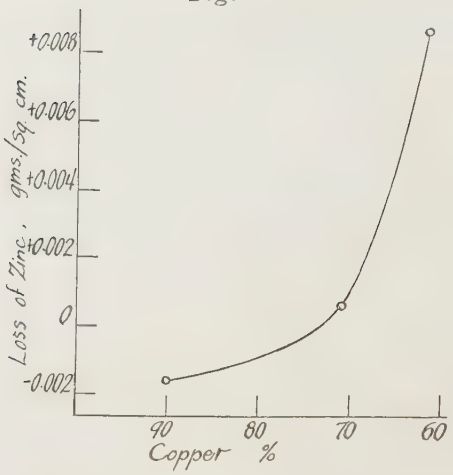

This experiment shows that zinc diffuses in or out of brass according to the vapour pressure of zinc in the surrounding medium, so the values given in Table VI and Fig. 6 will vary according to the temperature and duration of heating.

Table VII

Copper Content in %	Temp. °C.	$1/T \times 10^3$	Weight of Specimen in gms.	Surface Area of Specimen in sq. cms.	Weight-decrease		log ΔW
					in gms.	in gms./sq. cm. ΔW	
	905	.8489	3.4996	3.04	0.0796	0.0262	$\bar{2}.4180$
	900	.8525	3.5380	3.07	0.0847	0.0276	$\bar{2}.4407$
	850	.8905	3.9490	3.29	0.0730	0.0222	$\bar{2}.3461$
	822	.9132	3.5028	3.04	0.0524	0.0172	$\bar{2}.2365$
71.6	787	.9434	3.5956	3.09	0.0292	0.0094	$\bar{3}.9754$
	750	.9775	3.6114	3.11	0.0174	0.0056	$\bar{3}.7478$
	715	1.0121	3.0313	2.80	0.0082	0.0029	$\bar{3}.4667$
	714	1.0132	3.4151	3.02	0.0086	0.0028	$\bar{3}.4545$
	667	1.0638	3.3951	3.03	0.0044	0.0015	$\bar{3}.1620$
	640	1.0953	3.8602	3.25	0.0028	0.0009	$\bar{4}.9353$
	891	.8591	3.9679	3.36	0.1049	0.0312	$\bar{2}.4944$
	850	.8905	3.7576	3.25	0.0934	0.0287	$\bar{2}.4585$
68.6	812	.9217	3.7832	3.24	0.0555	0.0171	$\bar{2}.2337$
	773	.9579	3.1958	2.90	0.0256	0.0088	$\bar{3}.9458$
	735	.9921	3.4226	3.04	0.0138	0.0045	$\bar{3}.6570$
	699	1.0288	3.5674	3.14	0.0091	0.0029	$\bar{3}.4621$
	664	1.0673	3.7900	3.24	0.0050	0.0015	$\bar{3}.1884$

Table VII Continued

Copper Content in %	Temp. °C	$1/T \times 10^3$	Weight of Specimen in gms.	Surface Area of Specimen in sq. cms.	Weight-decrease		log ΔW
					in gms.	ingms./sq. cm. ΔW	
66.7	841	.8977	3.6095	3.24	0.1019	0.0315	$\bar{2}.4976$
	790	.9407	3.3202	3.00	0.0403	0.0134	$\bar{2}.1282$
	740	.9872	3.5324	3.14	0.0176	0.0056	$\bar{3}.7486$
	690	1.0384	3.4711	3.10	0.0097	0.0031	$\bar{3}.4954$
	650	1.0834	3.2308	3.01	0.0053	0.0018	$\bar{3}.2457$
65.0	841	.8977	3.6276	3.24	0.1158	0.0357	$\bar{2}.5532$
	795	.9363	3.6256	3.22	0.0560	0.0174	$\bar{2}.2403$
	768	.9606	3.6655	3.19	0.0346	0.0108	$\bar{2}.0353$
	741	.9862	3.5306	3.12	0.0225	0.0072	$\bar{3}.8580$
	713	1.0142	3.3962	3.11	0.0172	0.0055	$\bar{3}.7428$
	693	1.0352	3.5388	3.12	0.0134	0.0043	$\bar{3}.6330$
	657	1.0753	3.2024	2.94	0.0072	0.0024	$\bar{3}.3890$
63.6	847	.8929	3.7078	3.21	0.1056	0.0329	$\bar{2}.5172$
	797	.9346	3.4930	3.09	0.0564	0.0183	$\bar{2}.2613$
	750	.9775	3.1046	2.86	0.0267	0.0093	$\bar{3}.9701$
	704	1.0236	3.3050	2.99	0.0155	0.0052	$\bar{3}.7147$
	654	1.0787	3.4118	3.05	0.0070	0.0023	$\bar{3}.3608$
63.2	862	.881	3.8606	3.30	0.1050	0.0318	$\bar{2}.5027$
	807	.926	3.5965	3.22	0.0695	0.0216	$\bar{2}.3341$
	791	.9399	3.3012	2.97	0.0530	0.0178	$\bar{2}.2515$
	740	.9872	3.5711	3.13	0.0269	0.0086	$\bar{3}.9342$
	697	1.0309	3.1688	2.90	0.0138	0.0048	$\bar{3}.6775$
	661	1.0707	3.4845	3.09	0.0085	0.0028	$\bar{3}.4395$
59.9	850	.8905	3.6454	3.18	0.1426	0.0448	$\bar{2}.6517$
	800	.932	3.8533	3.30	0.0659	0.0200	$\bar{2}.3004$
	763	.9652	4.0782	3.43	0.0385	0.0112	$\bar{2}.0502$
	725	1.002	4.0666	3.43	0.0236	0.0069	$\bar{3}.8376$
	691	1.0373	3.7767	3.26	0.0151	0.0046	$\bar{3}.6658$
	653	1.0799	3.5616	3.14	0.0088	0.0028	$\bar{3}.4476$
59.2	851	.8897	3.6380	3.17	0.1644	0.0519	$\bar{2}.7148$
	816	.9191	3.6048	3.16	0.0935	0.0296	$\bar{2}.4711$
	775	.9542	3.2668	2.98	0.0492	0.0165	$\bar{2}.2178$
	739	.9881	3.4768	3.08	0.0264	0.0086	$\bar{3}.9331$
	711	1.0162	3.4089	3.04	0.0189	0.0062	$\bar{3}.7936$
	691	1.0373	3.5768	3.15	0.0157	0.0050	$\bar{3}.6976$
	665	1.066	3.2052	2.96	0.0103	0.0035	$\bar{3}.5406$
58.8	850	.8905	3.6023	3.17	0.1819	0.0521	$\bar{2}.7599$
	814	.9178	3.6740	3.20	0.1162	0.0363	$\bar{2}.5601$
	774	.9551	3.6445	3.19	0.0629	0.0197	$\bar{2}.2949$

Table VII Continued

Copper Content in %	Temp. °C	$1/T \times 10^3$	Weight of Specimen in gms.	Surface Area of Specimen in sq. cms.	Weight-decrease		log ΔW
					in gms.	in gms./sq. cm. ΔW	
5.88	751	.9716	3.3307	3.01	0.0380	0.0126	$\bar{2}.1012$
	730	.997	3.1477	2.92	0.0261	0.0089	$\bar{3}.9513$
	724	1.003	3.3896	3.03	0.0245	0.0081	$\bar{3}.9077$
	699	1.0289	3.1766	2.93	0.0172	0.0059	$\bar{3}.7687$
	668	1.0627	3.2564	3.04	0.0126	0.0041	$\bar{3}.6175$
50.6	839	.8993	3.5783	3.17	0.4225	0.1333	$\bar{1}.1248$
	801	.9311	3.9392	3.37	0.3033	0.0900	$\bar{2}.9542$
	773	.956	3.8321	3.34	0.2271	0.0680	$\bar{2}.8325$
	738	.9891	3.8707	3.34	0.1476	0.0442	$\bar{2}.6453$
	708	1.0194	3.7189	3.25	0.0960	0.0295	$\bar{2}.4704$
	704	1.0236	3.5948	3.18	0.0909	0.0286	$\bar{2}.4561$
	670	1.0605	3.6202	3.20	0.0506	0.0158	$\bar{2}.1990$
	665	1.0661	3.4971	3.12	0.0461	0.0148	$\bar{2}.1696$
	633	1.1037	3.6644	3.21	0.0289	0.0090	$\bar{3}.9544$
50.1	840	.8985	3.6858	3.25	0.4413	0.1358	$\bar{1}.1329$
	801	.9311	3.6460	3.23	0.2991	0.0926	$\bar{2}.9666$
	766	.9625	3.7650	3.26	0.2084	0.0639	$\bar{2}.8057$
	732	.995	3.6112	3.20	0.1312	0.0410	$\bar{2}.6128$
	693	1.0352	3.6304	3.23	0.0750	0.0232	$\bar{2}.3659$
	661	1.0707	3.5103	3.15	0.0495	0.0157	$\bar{2}.1963$
	660	1.0718	3.4826	3.13	0.0471	0.0150	$\bar{2}.1775$
	635	1.1013	3.5427	3.14	0.0259	0.0082	$\bar{3}.9164$

4. The Influence of Temperature

Specimens prepared from rods each of different composition were heated to 650—900°C. in a hydrogen atmosphere for 30 minutes; the results are shown summarised in Table VII.

Next, the specimen with 60.2 % Cu was annealed for 1.5 hours at 650°—670°C., its surface being covered with carbon to prevent change in the composition by volatilisation of zinc and oxidation. After being cooled in the furnace, it was machined and cut.

The results obtained with this specimen are given in Table VIII.

By plotting the logarithms of the amount of zinc lost, given in the last column of Tables VII and VIII, against the reciprocal of absolute temperature, two kinds of curves are obtained as shown in Fig. 7. The one kind consists of straight lines and the other shows break.

Table VIII

Temp. °C.	$1/T \times 10^3$	Weight of Specimen in gms.	Surface Area of Specimen in sq. cms.	Weight-decrease		log ΔW
				in gms.	in gms./sq. cm. ΔW	
855	0.8865	3.6755	3.20	0.1667	0.0521	$\bar{2}.7168$
801	0.9311	3.6110	3.17	0.0853	0.0269	$\bar{2}.4299$
755	0.9728	3.2326	3.05	0.0486	0.0159	$\bar{2}.2023$
714	1.0132	3.1680	2.96	0.0252	0.0085	$\bar{3}.9301$
673	1.0571	3.4162	3.04	0.0149	0.0049	$\bar{3}.6903$
630	1.1074	3.2917	3.00	0.0068	0.0023	$\bar{3}.3554$

Fig. 7

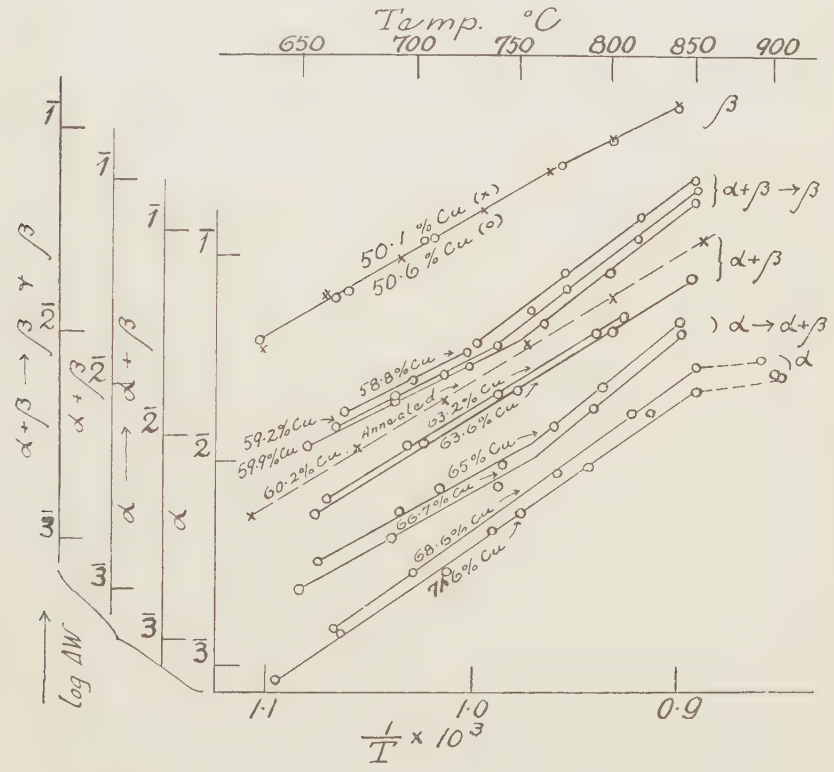

Comparing the above results with the equilibrium diagram of the Cu.–Zn system[1] lying between 70 % and 50 % Cu, Fig. 8, though

1. R. Genders and G. L. Bailey: Journ. Inst. Metals, **33**, 213 (1925).

the boundary lines between the α and $\alpha+\beta$ fields and the $\alpha+\beta$ and β fields vary to some extent according to the previous treatment of the alloys examined, the following facts are noticeable:—

Fig. 8

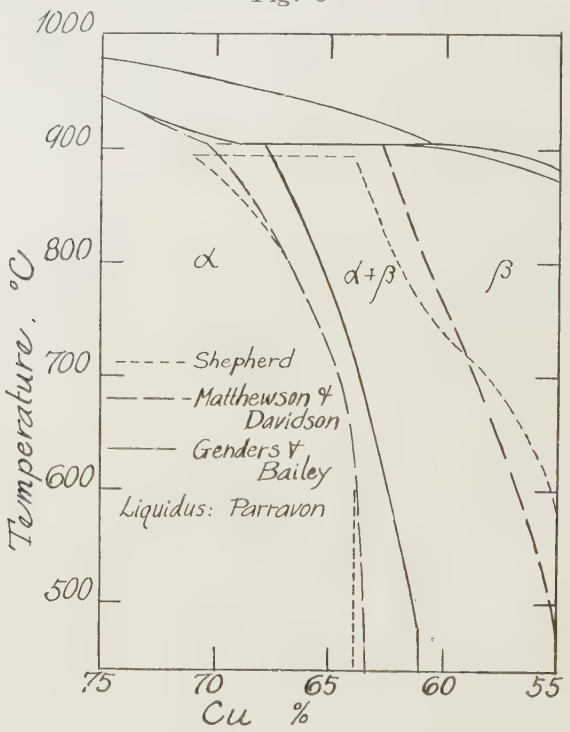

(1) Brasses whose composition corresponds to those which does not change their structural constituent within the experimental temperature range, show a relation represented by a straight line.

(2) The angle of inclination to the abscissa does not depend on the chemical composition but on the structural constituent; α brass being the largest, followed by $\alpha+\beta$ and β brass.

(3) With α brasses whose copper content is respectively 71.6 % and 68.7 %, the amount of zinc lost at 850° and 900°C. differs only a little. This could be explained if we were to find how the curve runs between these two temperatures by more experiments, but the present author could not do this owing to a lack of available specimens.

(4) In the case of brasses which change their structural constituent at some temperature within the experimental range, the line has a break at

the point approximately corresponding to the temperature at which this change occurs.

(5) In the case of brass which has α constituent at low temperatures, and $\alpha+\beta$ at high temperatures, both the parts corresponding to the α constituent stable at low temperatures and to the $\alpha+\beta$ stable at high temperatures do not run parallel respectively to that for brass of α constituent and that for brass of $\alpha+\beta$ constitusnt throughout the experimental range.

This phenomenon is probably due to the fact that the specimen retains to some extent the constituent stable at high temperatures because it is cast in an iron mould and subjected to relatively rapid cooling; it is also due to the fact that diffusion is aided by the distortion which occurs during the change of structural constituent

(6) The same relation holds in the case of the brasses which show $\alpha+\beta$ constituant at low temperatures and β at high temperatures.

In general, the relation between the amount of zinc lost per unit surface (ΔW) and the absolute temperature (T) may be expressed by the equation

$$\Delta W = A\, e^{-B/T}$$

where the constants A and B have a characteristic value depending on the structural constituents.

5. The Influence of Time

In order to study how the amount of zinc lost varies with the time, the following experiments were carried out:—

(1) Specimens of the same composition were heated at a definite temperature for period varying from 0.5 to 7.0 hours.

(2) A specimen was heated at a definite temperature for 45 minutes and the same operation was repeated ten times, the amount of zinc lost after each heating being measured.

Tables IX—XII and figs. 9 and 10 show the results.

Dunn[1] found that the amounts of zinc lost varied as the square root of the time with α brasses, in the form of a helical coil of wire, containing 9.58 % and 29.08 % Zn heated at 842°C. in vacuo. The above results, even those obtained with α brasses containing about 71 % Cu, do not agree with Dunn's.

1. J. S. Dunn: loc. cit.

Table IX

Weight of Specimen in gms.	Surface Area of Specimen in sq. cms.	Time of Heating in hrs.	Weight-decrease	
			in gms.	in gms./sq. cm.
Copper Content=61.1%: Temperature=850°C.				
3.7033	3.20	0.5	0.1683	0.0526
3.9576	3.35	0.5	0.1761	0.0526
3.7611	3.24	1.0	0.2913	0.0899
3.7700	3.25	1.5	0.4045	0.1245
3.5244	3.10	2.0	0.4676	0.1508
4.0058	3.38	2.5	0.5869	0.1736
3.5400	3.11	3.0	0.6128	0.1970
3.5449	3.12	3.0	0.6049	0.1939
3.3892	3.02	4.0	0.6754	0.2236
3.7956	3.27	5.0	0.8226	0.2516
3.3586	3.06	6.0	0.8050	0.2689
3.4256	3.11	7.0	0.8835	0.2841
Copper Content=62%: Temperature=794°C.				
3.7776	3.25	0.5	0.0560	0.0172
3.7937	3.25	1.0	0.1063	0.0327
3.6766	3.21	1.5	0.1516	0.0472
3.7086	3.21	2.0	0.1890	0.0589
3.6406	3.17	2.5	0.2362	0.0745
3.7652	3.23	3.0	0.2808	0.0889
3.5761	3.14	4.0	0.3365	0.1072
3.4844	3.09	5.0	0.3925	0.1270
3.4766	3.07	6.0	0.4288	0.1397
3.6110	3.16	6.0	0.4380	0.1386
3.7437	3.23	7.0	0.5094	0.1577
3.4607	3.06	7.0	0.4732	0.1546

Table X

Copper Content = 61.1 %
Temperature = 850°C.
Duration of each Heating = 45 mins.

Times of Heating	Weight-decrease after each Heating		Total Weight-decrease
	in gms.	in gms./sq. cm.	in gms./sq. cm.
Weight of Specimen = 3.7818gms.: Surface Area = 3.25 sq. cms.			
1	0.2384	0.0734	0.0734
2	0.1770	0.0558	0.1292
3	0.1367	0.0442	0.1734
4	0.1107	0.0363	0.2097
5	0.0817	0.0271	0.2368
6	0.0723	0.0245	0.2613
7	0.0682	0.0230	0.2843
8	0.0541	0.0185	0.3028
9	0.0481	0.0164	0.3192
10	0.0455	0.0159	0.3351
Surface Area after being treated = 2.878 sq. cms.			
Weight of Specimen = 3.4978 gms.: Surface Area = 3.086 sq. cms.			
1	0.2250	0.0729	0.0729
2	0.1732	0.0577	0.1306
3	0.1351	0.0459	0.1765
4	0.1065	0.0369	0.2134
5	0.0845	0.0296	0.2430
6	0.0713	0.0253	0.2683
7	0.0557	0.0200	0.2883
8	0.0481	0 0173	0.3056
9	0.0414	0.0151	0.3207
10	0.0363	0.0132	0.3339
Surface Area after being treated = 2.726 sq. cms.			

Table XI

Copper Content=71.2 %
Temperature=850°C.
Duration of each Heating=45 mins.
Weight of Specimen=3.6198 gms.
Surface Area=3.17 sq. cms.

Times of Heating	Weight-decrease after each Heating		Total Weight-decrease in gms./sq. cm.
	in gms.	in gms./sq. cm.	
1	0.1147	0.0362	0.0362
2	0.0817	0.0259	0.0621
3	0.0666	0.0213	0.0834
4	0.0582	0.0186	0.1020
5	0.0510	0.0164	0.1184
6	0.0459	0.0148	0.1332
7	0.0393	0.0137	0.1459
8	0.0351	0.0114	0.1573
9	0.0323	0.0105	0.1678
10	0.0282	0.0091	0.1769

Surface Area after being treated=3.07 sq. cms.

Table XII

Copper Content=71.6 %
Temperature=850°C.
Duration of each Heating=45 mins.
Weight of Specimen=3.5214 gms.
Surface Area=3.04 sq. cms.

Times of Heating	Weight-decrease after each Heating		Total Weight-decrease in gms./sq. cm.
	in gms.	in gms./sq. cm.	
1	0.1010	0.0332	0.0332
2	0.0728	0.0241	0.0573
3	0.0638	0.0212	0.0785
4	0.0502	0.0167	0.0952
5	0.0426	0.0143	0.1095
6	0.0420	0.0141	0.1236
7	0.0327	0.0110	0.1346
8	0.0302	0.0102	0.1448
9	0.0277	0.0093	0.1541
10	0.0264	0.0089	0.1630

Surface Area after being treated=2.954 sq. cms.

Fig. 9

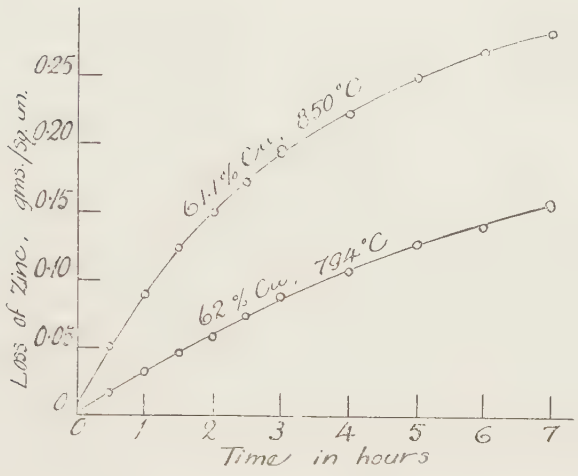
Loss of Zinc, gms./sq. cm.
0·25
0·20
0·15
0·10
0·05
0
61·1% Cu, 850°C
62 % Cu, 794°C
0 1 2 3 4 5 6 7
Time in hours

Fig. 10

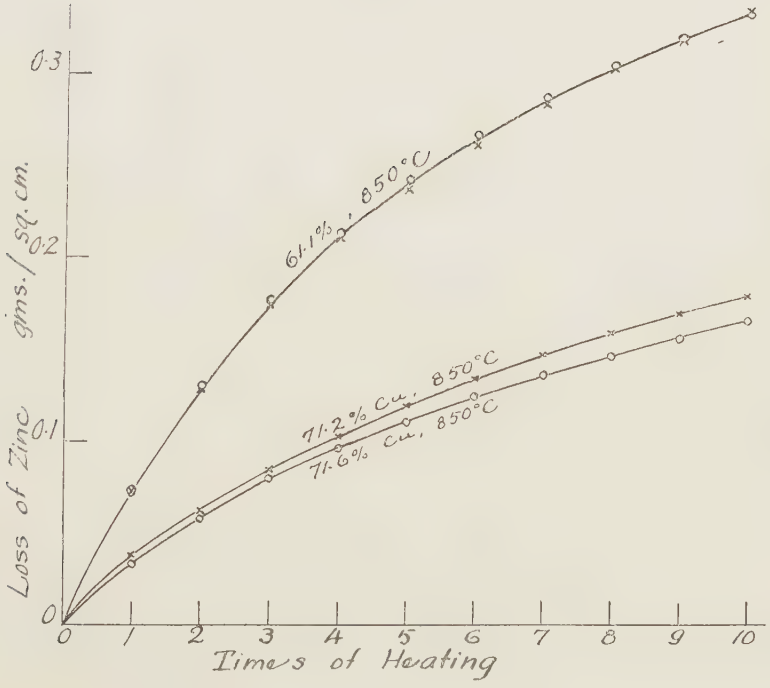
Loss of Zinc gms./sq. cm.
0·3
0·2
0·1
0
61·1% Cu, 850°C
71·2% Cu, 850°C
71·6% Cu, 850°C
0 1 2 3 4 5 6 7 8 9 10
Times of Heating

6. Appearance and Microstructure

When brass is heated in a hydrogen atmosphere, it changes colour on the surface, according to the amount of zinc lost, till it looks like pure copper, and shrinks. If the specimen is cylindrical in form, its length as well as its diameter show a greater shrinkage at the periphery than at the centre on account of the vaporisation of zinc being great there.

Brass increases in density with decreasing zinc content, but in this case its density decreases through the giving off of zinc, as is shown in the following results obtained with brass containing 61.1 % Cu, heated ten times for 45 minutes at 850°C.

	Before Treatment		After Treatment	
	1	2	1	2
Weight in gms.	3.4978	3.7818	2.5206	2.7491
Volume in cb. cms.	0.416	0.450	0.346	0.375
Density	8.40	8.41	7.30	7.34

Specimens with 65 % and 66.7 % Cu respectively have α structure regardless of the temperature at which they are heated. Photos. A_1, A_2 and A_3 show respectively the microstructure of specimens with 63.6 % Cu as cast and after being heated at 654° and 847°C. for 30 minutes. In A_2, it seems nearly homogeneous because the specimen was annealed to some extent by heating at 654°C. for 30 minutes; in A_3, β crystals are still observed at the central part notwithstanding that about 8 % of the total zinc is lost. The microstructure of annealed specimens with 60.2 % Cu (B_1, B_2 and B_3) and that of specimens with 58.8 % Cu (D_1, D_2 and D_3) show that crystalline grains grow as they are heated at high temperatures. The specimens as cast respectively with 50.1 % and 50.6 % Cu show a homogeneous structure (F_1 and E_1). In the case of those heated at high temperatures, however, the α crystals become more and more numerous near the surface (F_3 and E_3).

III. Experiments with Special Brass

In order to study the effect of a third element added to the ordinary brass on the vaporisation of zinc at high temperatures, the following experiments were carried out:—

1. Specimen

Up to 2 % of lead, tin, iron, manganese or aluminium was added to brasses containing copper and zinc in the ratio of approximately 6 : 4 and 7 : 3 respectively.

Table XIII shows the result of analysis of the specimens prepared and Table XIV that of the brasses used with these specimens for comparison.

Table XIII

No. of specimen	A (Pb)		B (Sn)		C (Fe)		D (Mn)		E (Al)	
	Cu %	Pb %	Cu %	Sn %	Cu %	Fe %	Cu %	Mn %	Cu %	Al %
1	70.82	0.16	70.82	0.25	69.92	0.31	70.42	0.22	70.22	0.22
2	69.82	0.34	70.61	0.53	68.21	0.55	70.22	0.54	70.32	0.78
3	69.62	0.65	69.62	0.98	71.02	1.03	70.61	0.80	69.31	1.12
4	69.12	1.09	66.33	1.97	70.61	2.25	65.77	1.96	67.81	2.10
5	59.67	0.20	61.56	0.24	58.95	0.32	60.56	0.31	60.60	0.19
6	59.96	0.32	60.96	0.56	58.35	0.58	60.25	0.48	60.96	0.61
7	59.15	0.66	59.96	1.15	59.55	1.14	60.15	0.85	60.76	1.25
8	58.55	1.37	57.54	2.13	57.95	2.21			59.77	2.13

Table XIV

No. of Specimen	Cu-content in %	Remarks
I	71.42	Heated with Specimens 1, 2, 3 and 4 in Tab. XIII at 600°C.
II	70.62	„ „ „ „ „ „ „ „ „ „ „ „ 700°C.
III	70.62	„ „ „ „ „ „ „ „ „ „ „ „ 800°C.
IV	59.76	Heated with Specimens 5, 6, 7 and 8 in Tab. XIII at 600°C.
V	60.56	„ „ „ „ „ „ „ „ „ „ „ „ 700°C.
VI	60.56	„ „ „ „ „ „ „ „ „ „ „ „ 800°C.

2. Experimental Procedure

Five specimens having the composition given in the same line in Table XIII and the corresponding brass given in Table XIV were

placed in a row in a porcelain boat, which was covered with a sheet of copper plate in order to maintain it at a uniform temperature, and heated in vacuo as well as in hydrogen at 600°, 700° and 800°C. for one hour.

3. Experiments carried out in Vacuo

The results obtained with the specimens containing 70 % copper are given in Table XV and are shown graphically in Fig. 11, and those with the specimens containing 60 % copper in Table XVI and in Fig. 12. In these tables, the data are given in terms of the ratio of the amount of zinc lost per unit surface of the specimen to that of the brass used for comparison. The variation of the latter with temperature is given in Fig. 13 in the case of brass containing 70 % copper and in Fig. 14 in the case of that containing 60 % copper.

Fig. 11

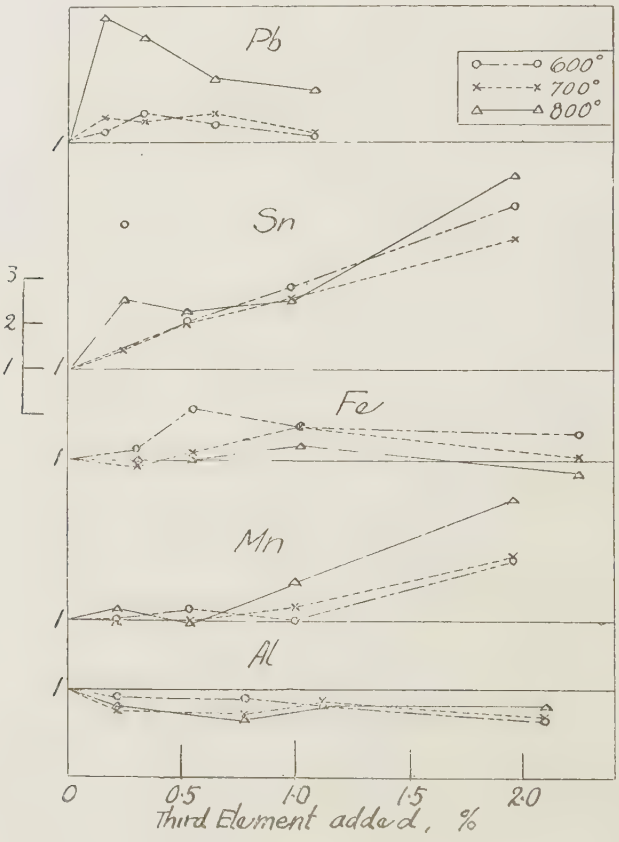

Table XV

Temp. °C.	No. of Specimen	Loss of Zinc, taking that from Brass used for Comparison as Unit					No. of Brass used for Comparison
		A (Pb)	B (Sn)	C (Fe)	D (Mn)	E (Al)	
600	1	1.20	4.19	1.24	1.02	0.85	I
	2	1.62	2.05	2.13	1.23	0.81	
	3	1.36	2.78	1.75	1.00	0.66	
	4	1.09	4.56	1.57	2.33	0.36	
700	1	1.53	1.41	0.87	0.98	0.49	II
	2	1.45	2.23	1.17	1.01	0.46	
	3	1.63	2.57	1.74	1.30	0.78	
		1.67*	2.68*	1.61*	1.41*	0.49*	
	4	1.20	3.88	1.08	2.41	0.41	
800	1	3.75	2.52	0.99	1.24	0.61	III
	2	3.31	1.98	1.01	0.94	0.36	
	3	2.38	2.49	1.31	1.85	0.63	
	4	2.13	5.26	0.72	3.64	0.65	

* The results obtained by changing the order of specimens in a boat.

Table XVI

Temp. °C.	No. of Specimen	Loss of Zinc, taking that from Brass used for Comparison as Unit					No. of Brass used for Comparison
		A (Pb)	B (Sn)	C (Fe)	D (Mn)	E (Al)	
600	5	1.09	1.06	1.05	0.83	0.62	IV
	6	0.67	1.23	1.65	0.85	0.46	
	7	0.69	1.63	1.09	0.91	0.78	
	8	0.49	3.78	1.24		2.01	
700	5	1.20	1.10	1.35	0.98	0.90	V
	6	1.13	1.15	1.64	0.91	0.85	
	7	1.17	1.32	1.17	0.86	0.84	
	8	1.03	2.80	1.21		1.56	
800	5	1.24	0.90	1.35	0.97	1.05	VI
	6	1.17	1.05	1.31	0.91	0.96	
	7	1.13	1.36	1.20	0.75	1.00	
	8	1.09	2.04	1.07		1.16	

Fig. 12

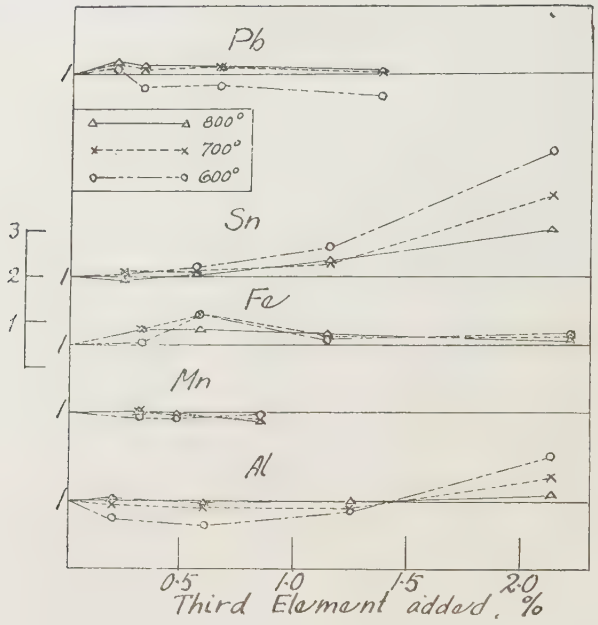

Fig. 13

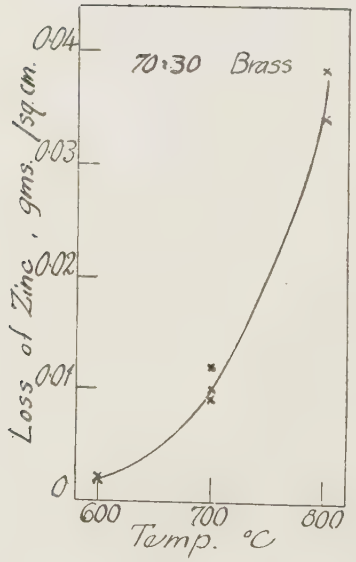

Fig. 14

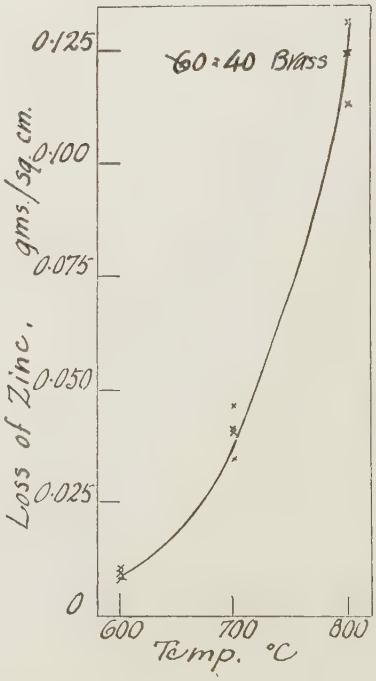

From the results obtained with specimens containing 70 % of copper, the following facts are deduced :—

(1) The loss of zinc increases with the addition of lead, which is intensified as the temperature to which the alloy is heated increases, but the amount of lead added seems not to have an appreciable influence.

(2) Tin promotes the evaporation of zinc most effectively and this effect becomes more marked the more tin is added.

(3) Iron also increases the loss of zinc but its effect becomes less at high temperatures, forming a contrast to lead.

(4) Manganese increases the loss of zinc though to a small extent than the former three elements.

(5) Aluminium, on the contrary, reduces the evaporation of zinc almost by half in all cases.

(6) The great values obtained with specimen containing 1.97 % of Sn and that containing 1.96 % of Al are partly due to their zinc content greater than that of the brass used for comparison (see Table XIII).

In the case of the specimens containing about 60 % of copper, the effects of adding a third element are not so marked as in the case of those with about 70 % copper.

Lead retards the evaporation of zinc at 600°C. and manganese at all temperatures, while aluminium promotes it at 800°C.

4. Experiments carried out in Hydrogen Atmosphere

As the amount of evaporation of zinc is very small at 600°C. in this case, only the results of experiments at 700° and 800°C. are given in Table XVII and are shown graphically, in Fig. 15 with specimens containing 70 % of copper, and in Fig. 16 with those containing 60 % of copper in the same way as those in vacuo.

The same specimens generally show lower values in this case than in the previous one, but the general features of the curves in Figs. 15 and 16 are similar to those in Figs. 11 and 12 respectively.

5. Relation between Loss of Zinc and Temperature

The relation between the loss of zinc and temperature was examined by plotting the logarithm of the former ($\log \Delta W$) against the reciprocal of absolute temperature ($1/T$). Examples are shown in

Table XVII

Temp. °C.	No. of Specimen	Loss of Zinc, taking that from Brass used for Comparison as Unit					No. of Brass used for Comparison
		A (Pb)	B (Sn)	C (Fe)	D (Mn)	E (Al)	
Cu and Zn are at the ratio of 70 to 30.							
700	1	1.17		0.88	0.93	0.61	II
	2	1.08	1.14	0.92	0.57	0.73	
	3	0.98	1.66	0.59	0.66	0.68	
	4	0.83	4.69	0.90	2.07	0.08	
800	1						III
	2	1.61	1.55	1.41	1.15	0.62	
	3	1.45	1.70	0.74	0.85	0.36	
	4	1.24	4.35	0.52	2.20	1.16	
Cu and Zn are at the ratio of 60 to 40.							
700	5	0.74	0.64	0.33	0.58	0.21	V
	6	0.91	0.76	1.53	0.58	0.34	
	7	0.46	0.99	0.70	0.41	0.32	
	8	0.67	3.88	0.61		0.13	
800	5	1.14	0.47	1.28	0.57	0.36	VI
	6	0.92	0.83	1.51	0.69	0.19	
	7	0.85	1.09	1.13	0.56	1.13	
	8	0.83	2.57	1.12		0.95	

Fig. 15

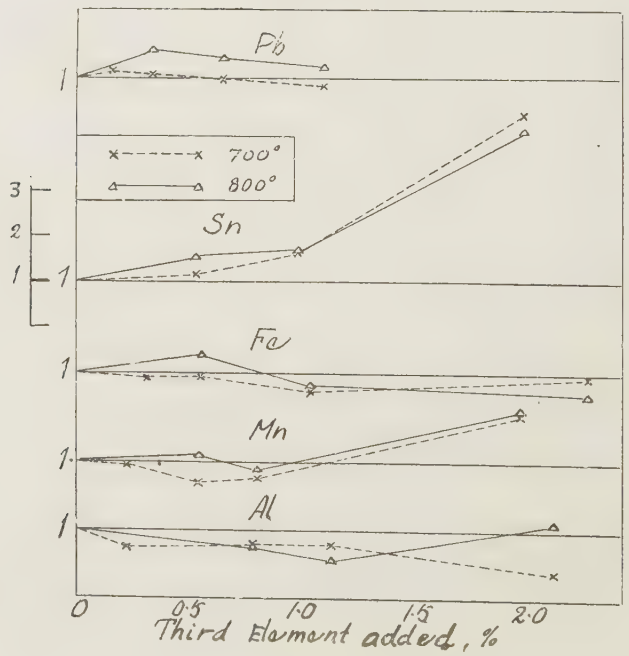

Fig. 16

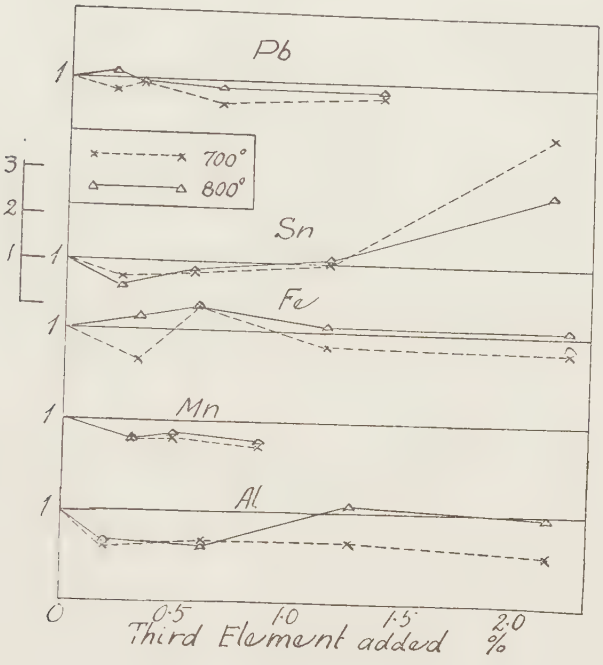
Pb
Sn
Fe
Mn
Al
700°
800°
3
2
1
0
0·5
1·0
1·5
2·0
Third Element added %

Fig. 17

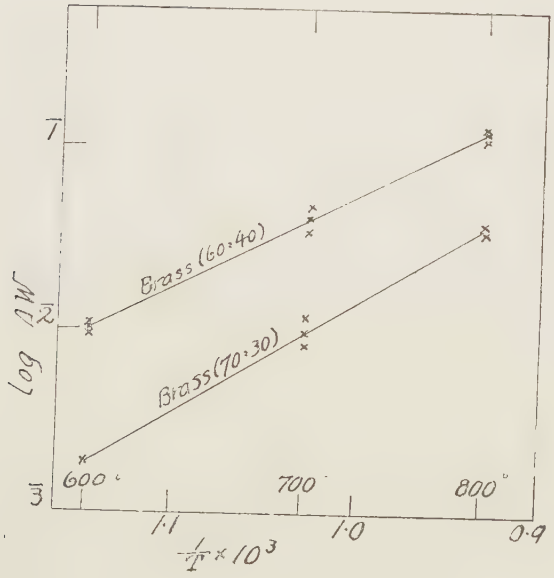
Brass (60:40)
Brass (70:30)
Log ΔW
600°
700°
800°
1·1
1·0
0·9
$\frac{1}{T} \times 10^3$

Fig. 18

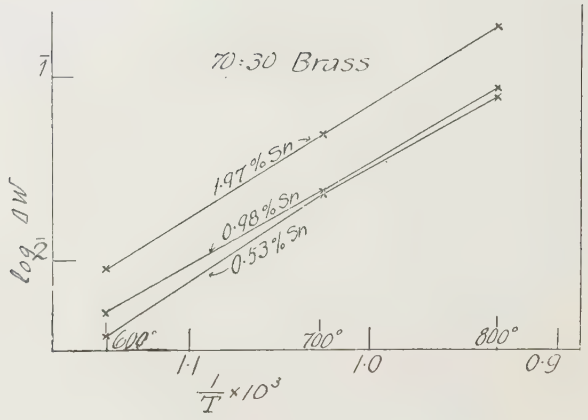

Fig. 19

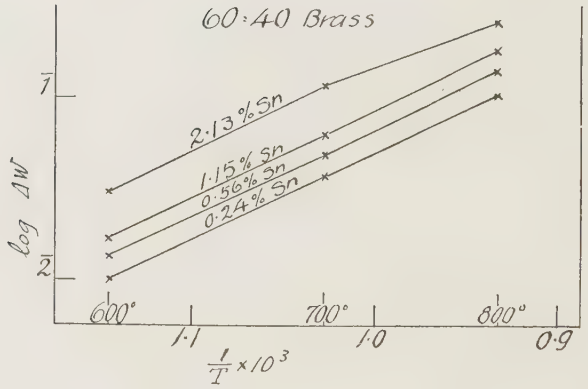

Fig. 17 with the brasses used for comparison and in Fig. 18 and Fig. 19 with those containing tin.

Though the duration of heating is long, fairly straight lines are obtained with plain brasses; the special brasses containing tin, however, show some irregularity. The other special brasses behave almost in the same manner.

Summary

1. By heating copper in contact with zinc vapour in a hydrogen atmosphere, the penetration of copper by zinc was studied with reference to the influence of temperature and time.

2. The loss of zinc from the surface of heated brasses ranging over the α, $\alpha+\beta$ and β fields was also studied with reference to the influence of composition, temperature and time.

3. The empirical formulas for the relation between the amount of zinc diffused into or out of copper and temperature, as well as for that between the loss of zinc from a heated brass surface and the composition, were established.

4. The effect of the addition to the brass of up to 2 % of third elements (lead, tin, iron, manganese and aluminium) on the evaporation of zinc from the brass at 600°, 700° and 800°C. in vacuo as well as in hydrogen was studied.

In conclusion, the author desires to express his sincere thanks to Prof. Dr. M. Chikashige, Director of the Institute, for his encouragement throughout the course of this work.

Institute for Chemical Research,
Imperial University, Kyoto.

Plate I

No. 1

Cu treated three times at 500°C. for 30 mins. with a gain of 0.0325 gm. Zn per sq. cm.

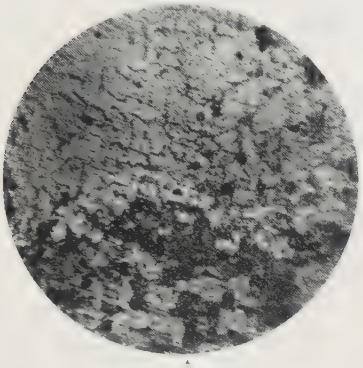

Edge

No. 2

Cu treated at 600°C. for 30 mins. with a gain of 0.0780 gm. Zn per sq. cm.

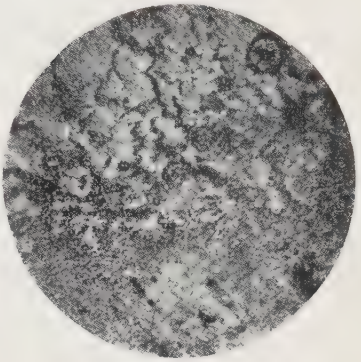

Edge

63.6 % Cu

A_1

As cast

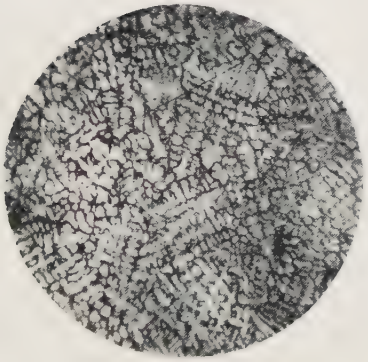

A_2

Heated at 654°C. for 30 mins.

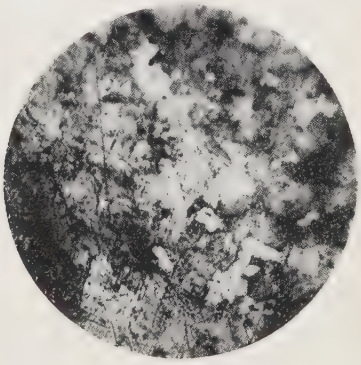

A_3

Heated at 847°C. for 30 mins.

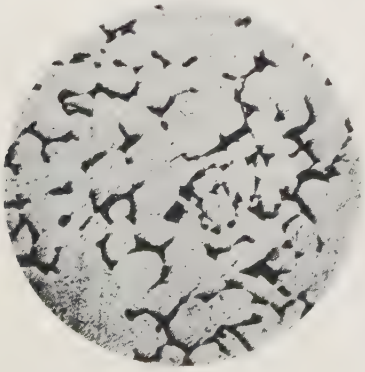

Plate II

60.2 % Cu

Annealed for 1.5 hrs. at 650—670°C.

B_1
As annealed

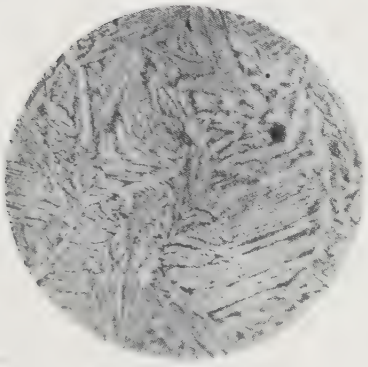

B_2
Heated at 630°C.
for 30 mins.

B_3
Heated at 855°C.
for 30 mins.

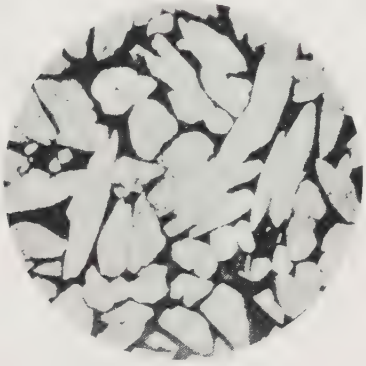

59.2 % Cu

C_2
Heated at 665°C.
for 30 mins.

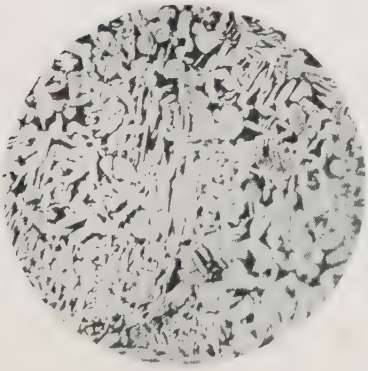

C_3
Heated at 851°C.
for 30 mins.

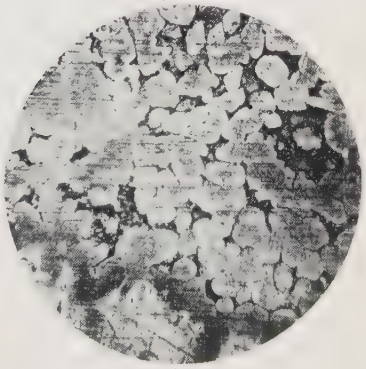

↑
Edge

Plate III

58.8 % Cu

D_1

As cast

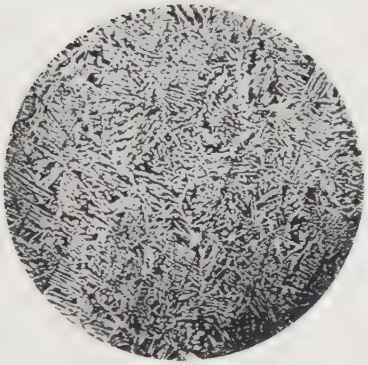

D_2

Heated at 668°C.
for 30 mins.

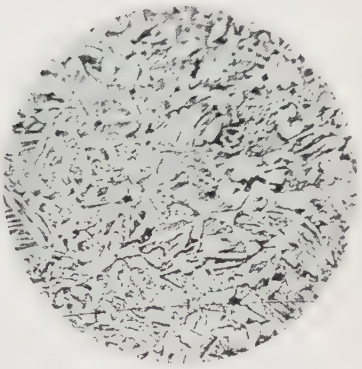

D_3

Heated at 850°C.
for 30 mins.

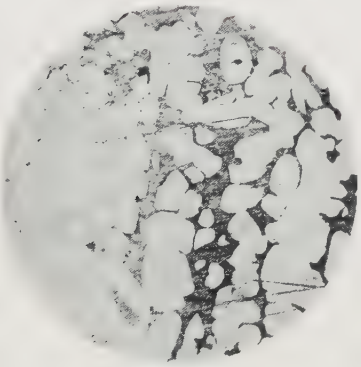

Plate IV

50.6 % Cu

E_1

As cast

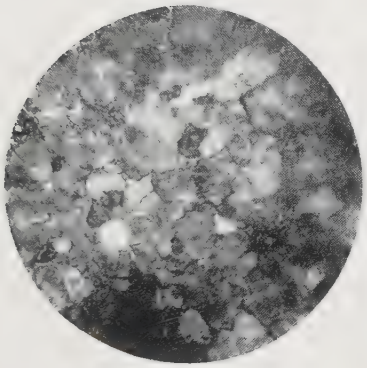

E_2

Heated at 663°C.
for 30 mins.

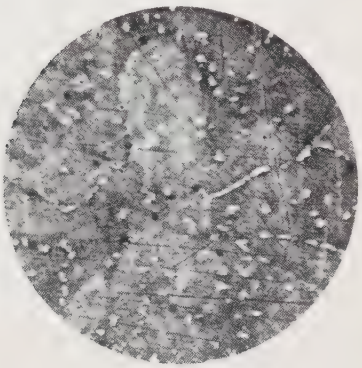

E_3

Heated at 839°C.
for 30 mins.

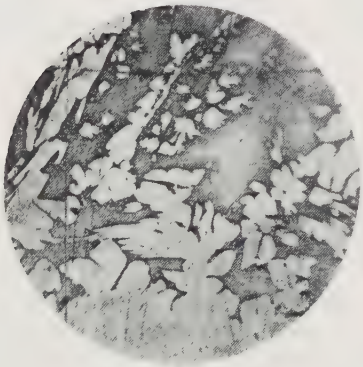

Edge

Plate V

50.1 % Cu

F_1

As cast

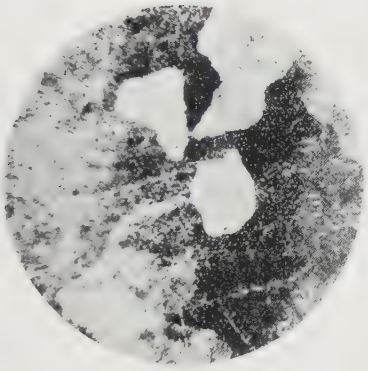

F_2

Heated at 660°C.
for 30 mins.

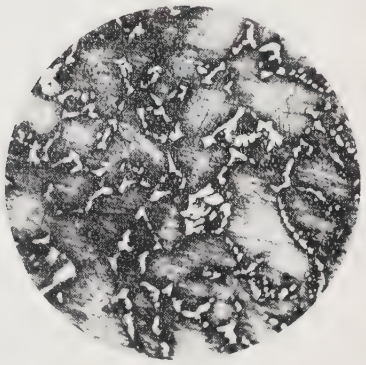

F_3

Heated at 840°C.
for 30 mins.

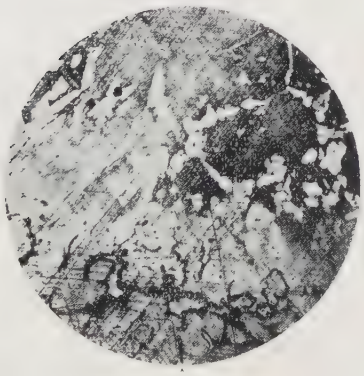

Edge

On the Solutions of the Cosmological Field Equations and Some Models of the Universe with Annihilation of Matter

By

Shujiro Kunii

(Received January 16, 1932)

Abstract

The aim of this paper is to classify all the possible solutions for relativistic cosmology and to construct a reasonable model of our actual universe. Using the line element

$$ds^2=-R(t)^2\{d\vartheta^2+\sin^2\vartheta d\varphi^2+\sin^2\vartheta\sin^2\varphi d\psi^2\}+F(\vartheta,t)^2\,dt^2,$$

the writer shows that the solutions of the amplified field-equations may be separated into two groups i. e. $\dot{R}=0$ and $\frac{\partial F}{\partial\vartheta}=0$. The former gives Einstein's and de Sitter's world, while the latter gives a unique solution when the pressure p vanishes, and many different solutions when p does not vanish. Important properties of a non-statical world, such as motion of a particle, Doppler shift and the form of the universe at eternity are described in § 4 and § 5. In the last section the writer introduces a new model of the universe and discusses its properties and then estimates the initial and present radius of that world.

One of the most interesting attempts in the general theory of relativity is to consider the shape and size of our universe as a whole. The inadequacy of interpreting our actual universe by Einstein's cylindrical or de Sitter's spherical world has come to be generally recognised. Many relativitists are inclined to consider our universe as a non-statical rather than a statical world on account of valuable contributions due to American astrophysicists. Adopting

$$ds^2=-\frac{e^{\sigma(t)}}{\left(1+\frac{r^2}{4R^2}\right)^2}(dx^2+dy^2+dz^2)+dt^2$$

as the line-element of our non-statical world, they[1] attempted to in-

1. R. C. Tolman: Proc. Nat. Acad. Sci., **16**, 320, 409, 511 (1930).
W. de Sitter: Proc. Nat. Acad. Sci., **16**, 474 (1930).
T. Takéuchi: Proc. Phys. Math. Soc. Jap., **13**, 166 (1931).

terpret many important observational facts, for example the correlation between distances and radial velocities of extragalactic nebulae, as the necessary consequences of our space-time world.

In the present paper, starting from a more general line-element for the universe, the writer tries first to show systematically how many solutions are possible for the cosmological problem, next to study what properties they have and finally to give a new model having reasonable properties in many respects.

§ 1. Field-equations with λ-term.

We assume that in our world at large there exist coordinate systems for which the forward velocity of light along any track is equal to the backward velocity along the same track and the 3-spaces are homogeneous and isotropic with respect to space-like coordinates. If $(\vartheta, \varphi, \psi, t)$ be a coordinate system having these properties, the line-element of our world can be written in the form

$$ds^2 = -R(t)^2\{d\vartheta^2 + \sin^2\vartheta d\varphi^2 + \sin^2\vartheta\sin^2\varphi d\psi^2\} + F(\vartheta, t)^2\, dt^2. \quad (1\cdot1)$$

From (1·1) it is obvious that our coordinate hypersurfaces form a 4-tuply orthogonal system. Accordingly we can find the Riemann-tensor R_{hijk} of our world by means of the well-known formulae[1]. Among 20 independent components of R_{hijk}, we obtain

$$\left.\begin{aligned}
R_{2112} &= R^2\sin^2\vartheta\left\{1 + \left(\frac{\dot R}{F}\right)^2\right\},\\
R_{3113} &= R^2\sin^2\vartheta\sin^2\varphi\left\{1 + \left(\frac{\dot R}{F}\right)^2\right\},\\
R_{4114} &= RF\left\{\frac{1}{R}\frac{\partial^2 F}{\partial\vartheta^2} - \frac{\partial}{\partial t}\left(\frac{\dot R}{F}\right)\right\},\\
R_{3223} &= R^2\sin^4\vartheta\sin^2\varphi\left\{1 + \left(\frac{\dot R}{F}\right)^2\right\},\\
R_{4224} &= RF\sin\vartheta\left\{\frac{1}{R}\frac{\partial F}{\partial\vartheta}\cos\vartheta - \frac{\partial}{\partial t}\left(\frac{\dot R}{F}\right)\sin\vartheta\right\},\\
R_{4334} &= RF\sin\vartheta\sin^2\varphi\left\{\frac{1}{R}\frac{\partial F}{\partial\vartheta}\cos\vartheta - \frac{\partial}{\partial t}\left(\frac{\dot R}{F}\right)\sin\vartheta\right\},\\
R_{1221} &= \frac{R\dot R}{F}\frac{\partial F}{\partial\vartheta}\sin^2\vartheta,\\
R_{1334} &= \frac{R\dot R}{F}\frac{\partial F}{\partial\vartheta}\sin^2\vartheta\sin^2\varphi,
\end{aligned}\right\} \quad (1\cdot2)$$

1. L. P. Eisenhart: Riemannian geometry, p. 119. (1926).

as non-vanishing components, where R, F and $\dot{R}$ are the abridged notations of $R(t)$, $F(\vartheta, t)$ and $\frac{dR}{dt}$ respectively.

Moreover we may assume that in our coordinate system the energy-momentum tensor T_{ij} which occurs in the Einstein's field-equations with λ-term, i. e.

$$G_{ij}-\lambda g_{ij}=-\varkappa\left(T_{ij}-\frac{1}{2}g_{ij}T\right), \tag{1·3}$$

is given by the following scheme

$$\begin{matrix} T_{ij}= & -p g_{11} & 0 & 0 & 0 \\ & 0 & -p g_{22} & 0 & 0 \\ & 0 & 0 & -p g_{33} & 0 \\ & 0 & 0 & 0 & g_{44}(\rho_0+3p), \end{matrix} \tag{1·4}$$

where both the pressure p and the microscopic density of matter ρ_0 are functions of t only according to the spacial homogeneity of our world. If we calculate G_{ij} by (1·1) and (1·2) and apply these values of G_{ij} and (1·4) to (1·3), we obtain

$$G_{11}=-2\left\{1+\left(\frac{\dot{R}}{F}\right)^2\right\}+\frac{R}{F}\left\{\frac{1}{R}\frac{\partial^2 F}{\partial\vartheta^2}-\frac{\partial}{\partial t}\left(\frac{\dot{R}}{F}\right)\right\}$$

$$=-R^2\left\{\lambda+\varkappa p+\frac{\varkappa\rho_0}{2}\right\}, \tag{1·5}$$

$$G_{22}=\frac{1}{F}\frac{\partial F}{\partial\vartheta}\sin\vartheta\cos\vartheta-\sin^2\vartheta\left[2\left\{1+\left(\frac{\dot{R}}{F}\right)^2\right\}\right.$$

$$\left.+\frac{R}{F}\frac{\partial}{\partial t}\left(\frac{\dot{R}}{F}\right)\right]=-R^2\sin^2\vartheta\left\{\lambda+\varkappa p+\frac{\varkappa\rho_0}{2}\right\}, \tag{1·6}$$

$$G_{44}=-\frac{F}{R}\left[\frac{1}{R}\frac{\partial^2 F}{\partial\vartheta^2}-\frac{\partial}{\partial t}\left(\frac{\dot{R}}{F}\right)+\frac{2}{\sin\vartheta}\left\{\frac{1}{R}\frac{\partial F}{\partial\vartheta}\cos\vartheta\right.\right.$$

$$\left.\left.-\frac{\partial}{\partial t}\left(\frac{\dot{R}}{F}\right)\sin\vartheta\right\}\right]=F^2\left\{\lambda-3\varkappa p-\frac{\varkappa\rho_0}{2}\right\}, \tag{1·7}$$

$$G_{14}=-2\frac{\dot{R}}{FR}\frac{\partial F}{\partial\vartheta}=0, \tag{1·8}$$

as the independent equations to be solved. From (1·8) it follows that the solutions of our problem can be classified into two groups :—
(I) $\dot{R}=0$, i. e. statical solutions in which R takes a constant value, say R_0.

(II) $\frac{\partial F}{\partial \vartheta}=0$, i. e. solutions in which we may put $F=1$ without loss of generality.

In accordance with this important result, we shall treat these two solutions separately.

§ 2. Statical solutions; $R=R_0$.

In this article we shall consider the statical solutions i. e. $R=R_0$. Thus the field-equations (1·5), (1·6) and (1·7) can be reduced to

$$\frac{1}{F}\frac{\partial^2 F}{\partial \vartheta^2}-2=-R_0^2\left(\lambda+\varkappa p+\frac{\varkappa\rho_0}{2}\right) \tag{2·1}$$

$$\frac{1}{F}\frac{\partial F}{\partial \vartheta}\sin\vartheta\cos\vartheta-2\sin^2\vartheta=-R_0^2\sin^2\vartheta\left(\lambda+\varkappa p+\frac{\varkappa\rho_0}{2}\right) \tag{2·2}$$

$$\frac{1}{R_0^2}\frac{\partial^2 F}{\partial \vartheta^2}+\frac{2}{R_0^2}\frac{\partial F}{\partial \vartheta}\cot\vartheta=-F\left(\lambda-3\varkappa p-\frac{\varkappa\rho_0}{2}\right). \tag{2·3}$$

Eliminating $\left(\lambda+\varkappa p+\frac{\varkappa\rho_0}{2}\right)$ between (2·1) and (2·2), we obtain

$$\frac{\partial^2 F}{\partial \vartheta^2}-\frac{\partial F}{\partial \vartheta}\cot\vartheta=0.$$

Hence we get

$$F=T_2(t)+T_1(t)\cos\vartheta, \tag{2·4}$$

$T_2(t)$ and $T_1(t)$ being arbitrary functions of t only. Eliminating ρ_0 between (2·1) and (2·3) and then applying (2·4) to it, we get

$$\left(\frac{1}{R_0^2}-\lambda+\varkappa p\right)T_2(t)+\left(\frac{3}{R_0^2}-\lambda+\varkappa p\right)T_1(t)\cos\vartheta=0.$$

From this it follows that the present case should be separable into two classes :—

(i) $T_1=0$ and $\frac{1}{R_0^2}=\lambda-\varkappa p$.

If we introduce $\int T_2(t)dt$ as a new coordinate and denote it by t, the line-element can be put in the form

$$ds^2=-R_0^2(d\vartheta^2+\sin^2\vartheta d\varphi^2+\sin^2\vartheta\sin^2\varphi d\psi^2)+dt^2 \tag{2·5}$$

and the relations connecting p, ρ_0, λ and R_0 are evidently

$$\left.\begin{aligned}\frac{1}{R_0^2}&=\lambda-\varkappa p,\\ \frac{2}{\varkappa R_0^2}&=4p+\rho_0.\end{aligned}\right\} \tag{2·6}$$

It is well known that this is nothing but Einstein's cylindrical world.

(ii) $T_2=0$ and $-\frac{3}{R_0^2}=\lambda-\varkappa p$.

If we introduce $\int T_1(t)dt$ as a new coordinate and denote it by t, the line-element can be written in the form

$$ds^2=-R_0^2(d\vartheta^2+\sin^2\vartheta d\varphi^2+\sin^2\vartheta\sin^2\varphi d\psi^2)+\cos^2\vartheta dt^2 \tag{2·7}$$

and the relations connecting p, ρ_0, λ and R_0 are obviously

$$\left.\begin{aligned}&-\frac{3}{R_0^2}=\lambda-\varkappa p,\\&4p+\rho_0=0.\end{aligned}\right\} \tag{2·8}$$

As is well known, this is de Sitter's spherical world.

According to our nomenclature, when $R(t)$ takes a constant value the world is said to be a statical one. Strictly speaking, it is a statical world with respect to the coordinate system $(\vartheta, \varphi, \psi, t)$. From the above consideration it will be seen that a statical world belongs either to Einstein's cylindrical world or to de Sitter's spherical world. This corresponds to the theorem independently obtained by Tolman[1] and Robertson[2].

§ 3. Non-statical solutions

Hereafter let us confine ourselves to the consideration of the case $F=1$. Thus the field equations (1·5), (1·6) and (1·7) are reducible to the form

$$\frac{2\ddot{R}}{R}+\frac{1+\dot{R}^2}{R^2}=\lambda-\varkappa p, \tag{3·1}$$

$$\frac{1+\dot{R}^2}{R^2}=\frac{1}{3}(\lambda+\varkappa\rho_0+3\varkappa p). \tag{3·2}$$

Putting

$$\rho=\rho_0+3p \tag{3·3}$$

and calling it the macroscopic density of energy, we can write it in the form

$$\rho=\frac{f(R)}{R^3}, \tag{3·4}$$

---

1. R. C. Tolman: Proc. Nat. Acad. Sci., **15**, 297 (1929).
2. H. P. Robertson: Proc. Nat. Acad. Sci., **15**, 822 (1929).

where $f(R)$ is a function of R yet unknown. Applying (3·4) to (3·2), we obtain

$$\dot{R}=\sqrt{\frac{\lambda}{3}R^2-1+\frac{\varkappa f(R)}{3R}}. \tag{3·5}$$

The reasons for rejecting the negative root will become clear later.

From (3·5), we get

$$t=\int_{R_0}^{R}\frac{dx}{\sqrt{\frac{\lambda}{3}x^2-1+\frac{\varkappa f(x)}{3x}}}, \tag{3·6}$$

R_0 being the initial value of R.

Differentiating (3·5) with respect to t and applying (3·1) and (3 5) to it, we obtain

$$p=-\frac{f'(R)}{3R^2}. \tag{3·7}$$

If we assume the 3-space to be elliptical, the total invariant mass of matter in the world M_0 is given by

$$M_0=\pi^2R^3\rho_0=\pi^2\{f(R)+Rf'(R)\}. \tag{3 8}$$

From what has been said, it is clearly convenient to discuss all the non-statical solutions separately according to the following classification.

(i) $p=0$, i. e. zero-pressure solutions. In this case, as will easily be seen from (3·7), $f(R)$ is a constant. Denoting it by $\frac{3A}{\varkappa}$, we have, by (3·8),

$$M_0=\frac{3A\pi^2}{\varkappa}. \tag{3 9}$$

In the zero-pressure universe the total invariant mass is necessarily constant.

(ii) $p\neq 0$. We can divide this case into two sub-classes.

(a) $M_0=$const. Denoting this constant by π^2D, (3·8) gives

$$f(R)+Rf'(R)=D.$$

Hence we get

$$f(R)=D+\frac{B}{R}, \tag{3·10}$$

where B is an integration constant.

(b) $M_0 \neq$ const. In this case, $f(R)$ is indeterminate.

§ 4. Some properties of a non-statical world.

Let us now consider the motion of a particle and the behaviour of light in a non-statical world. Without any loss of generality we may confine ourselves to the hypersurface $\varphi = \frac{\pi}{2}$, where the line element assumes the form

$$ds^2 = dt^2 - R(t)^2 \{d\vartheta^2 + \sin^2\vartheta d\psi^2\}. \tag{4·1}$$

(A) Motion of a particle.

Using the variational principle

$$\delta \int ds = 0$$

and (4·1), we find

$$\left.\begin{aligned} &\frac{d}{ds}(R^2 \sin^2\vartheta\, \psi') = 0, \\ &t'' + R\dot{R}(\vartheta'^2 + \sin^2\vartheta\, \psi'^2) = 0, \\ &R^2(\vartheta'^2 + \sin^2\vartheta\, \psi'^2) = t'^2 - 1, \end{aligned}\right\} \tag{4·2}$$

for the differential equations of the path, where the accent denotes $\frac{d}{ds}$. Eliminating t and s, the spacial path of the particle is determined by the differential equation

$$\frac{d^2\vartheta}{d\psi^2} - 2\cot\vartheta\left(\frac{d\vartheta}{d\psi}\right)^2 - \sin\vartheta\cos\vartheta = 0.$$

It can easily be shown that this defines a geodesic in the 3-space whose line element dl is given by

$$dl^2 = R(t)^2 (d\vartheta^2 + \sin^2\vartheta d\psi^2). \tag{4·3}$$

From the last two equations of (4 2), we obtain the first integral

$$ds = \frac{R dt}{\sqrt{a^2 + R^2}}, \tag{4·4}$$

where a is an integration constant and the positive sense of s is taken for the direction in which t increases. If we define the squared velocity v^2 of a particle by $\left(\frac{dl}{dt}\right)^2$, we find, from (4·1), (4·3) and (4·4),

$$v^2 = \left(\frac{dl}{dt}\right)^2 = \frac{a^2}{a^2 + R^2}. \tag{4·5}$$

Consequently the velocity of a free particle decreases only when $\dot{R}>0$. On the other hand, the velocity increases with time when $\dot{R}<0$, so that the stable model of the universe will not be obtained, as Tolman has pointed out.

(B) Behaviour of light.

By a slight modification of the argument given in (A), we can easily show that the spacial path of a light-ray is a geodesic in the 3-space $t=$const. Next let us suppose a light source situated in (ϑ_1, φ_1) at an instant t_1. At this moment the source sends a pair of light-signals separated by the time Δt_1, during which its position changes from (ϑ_1, φ_1) to $(\vartheta_1+\Delta\vartheta_1, \varphi_1+\Delta\varphi_1)$, to the stationary observer at the origin of the coordinate system. If t_2 and $t_2+\Delta t_2$ are respectively the instants receiving these signals, we have

$$\int_{t_1}^{t_2} \frac{dt}{R(t)} = \int_{(0,0)}^{(\vartheta_1, \varphi_1)} \sqrt{d\vartheta^2+\sin^2\vartheta d\varphi^2}$$

and

$$\int_{t_1+\Delta t_1}^{t_2+\Delta t_2} \frac{dt}{R(t)} = \int_{(0,0)}^{(\vartheta_1+\Delta\vartheta_1,\ \varphi_1+\Delta\varphi_1)} \sqrt{d\vartheta^2+\sin^2\vartheta d\varphi^2}\,.$$

Hence we get

$$\int_{t_2}^{t_2+\Delta t_2} - \int_{t_1}^{t_1+\Delta t_1} = \Delta\vartheta_1.$$

But, according to Einstein's principle of the permanence of atoms, this gives

$$\frac{\Lambda+\delta\Lambda}{\Lambda} = \frac{R(t_2)}{R(t_1)} \cdot \frac{1+(v_r)_1}{\left(\frac{ds}{dt}\right)_1},$$

where Λ and $\Lambda+\delta\Lambda$ are the wave-lengths of a definite line in the stellar and terrestrial spectrum and $(v_r)_1$ is the radial velocity of the source. Since the velocity v_1 of the source is given by

$$\left(\frac{ds}{dt}\right)_1^2 = 1 - v_1^2,$$

we obtain, from (4·6), the general formula for the Doppler-effect

$$V = \frac{\delta\Lambda}{\Lambda} = \frac{R(t_2)}{R(t_1)} \cdot \frac{1+(v_r)_1}{\sqrt{1-v_1^2}} - 1, \qquad (4\cdot7)$$

V being the radial velocity of the source. Neglecting v_1^2 for 1, (4·7) can be put in the form

$$V=\frac{R(t_2)}{R(t_1)}\{1+(v_r)_1\}-1. \tag{4·8}$$

Furthermore, if we neglect the proper motion of the source relative to our coordinate system, we finally get

$$V=\frac{R(t_2)}{R(t_1)}-1. \tag{4·9}$$

This shows us that $\dot{R}$ must be positive in order to interpret the red shift as the necessary consequence of our space-time world.

§ 5. Property of non-statical world when t tends to $+\infty$.

According to Riemannian geometry, the necessary and sufficient condition that a space V_n be of constant curvature K_0 is that the components of the fundamental tensor g_{ij} satisfy the conditions

$$R_{hijk}=K_0(g_{hj}g_{ik}-g_{hk}g_{ij}). \tag{5·1}$$

If we calculate R_{hijk} in order to apply this theorem to our non-statical world whose line element is given by

$$ds^2=-R(t)^2\{d\vartheta^2+\sin^2\vartheta d\varphi^2+\sin^2\vartheta\sin^2\varphi d\psi^2\}+dt^2,$$

we find, by (1·2)

$$\begin{aligned}
&R_{2112}=R^2\sin^2\vartheta(1+\dot{R}^2), && R_{3223}=R^2\sin^4\vartheta\sin^2\varphi(1+\dot{R}^2),\\
&R_{3113}=R^2\sin^2\vartheta\sin^2\varphi(1+\dot{R}^2), && R_{4224}=-R\ddot{R}\sin^2\vartheta,\\
&R_{4114}=-R\ddot{R}, && R_{4334}=-R\ddot{R}\sin^2\vartheta\sin^2\varphi,
\end{aligned}$$

for non-vanishing components. By means of (3·1), (3·2), (5·1) and these values of R_{hijk}, we find that the necessary and sufficient condition that our non-statical world be of constant curvature K_0 is that the ratios

$$\begin{aligned}
&\frac{R_{2112}}{g_{12}g_{12}-g_{11}g_{22}}=-\frac{1+\dot{R}^2}{R^2}=-\frac{\lambda}{3}-\frac{\varkappa\rho_0}{3}-\varkappa p,\\
&\frac{R_{3113}}{g_{13}g_{13}-g_{11}g_{33}}=-\frac{1+\dot{R}^2}{R^2}=-\frac{\lambda}{3}-\frac{\varkappa\rho_0}{3}-\varkappa p,\\
&\frac{R_{4114}}{g_{14}g_{14}-g_{11}g_{44}}=-\frac{\ddot{R}}{R}=-\frac{\lambda}{3}+\frac{\varkappa\rho_0}{6}+\varkappa p,\\
&\frac{R_{3223}}{g_{23}g_{23}-g_{22}g_{33}}=-\frac{1+\dot{R}^2}{R^2}=-\frac{\lambda}{3}-\frac{\varkappa\rho_0}{3}-\varkappa p,
\end{aligned} \tag{5·2}$$

$$\frac{R_{4224}}{g_{24}g_{24}-g_{22}g_{44}}=-\frac{\ddot{R}}{R}=-\frac{\lambda}{3}+\frac{\varkappa\rho_0}{6}+\varkappa p,$$
$$\frac{R_{4334}}{g_{34}g_{34}-g_{33}g_{44}}=-\frac{\ddot{R}}{K}=-\frac{\lambda}{3}+\frac{\varkappa\rho_0}{6}+\varkappa p,$$

must have the common value K_0. Hence if ρ_0 and p tend to zero when t tends to $+\infty$, all the ratios of the left-hand side in (5·2) converge to the limiting value $-\frac{\lambda}{3}$. Thus we have the theorem: The non-statical world such that its pressure and microscopic density of matter tend to zero when the time tends to positive infinity converges to the de Sitter's spherical world having $\sqrt{\frac{3}{\lambda}}$ as its curvature-radius if the time becomes positive infinity.

§ 6. Zero-pressure solution.

When $p=0$, from (3·6) and (3·9), the relation between R and t is given by the integral

$$t=\int_{R_0}^{R}\sqrt{\frac{x}{A-x+\frac{\lambda}{3}x^3}}\,dx, \tag{6·1}$$

where A is positive since M_0 must be positive. For simplicity we shall denote this integral by $I(R)$.

(a) Case: $A-\frac{2}{3\sqrt{\lambda}}>0$. $I(R)$ has a finite lower limit, because there exists no singularity in the integrand and R does not become negative.

(b) Case: $A-\frac{2}{3\sqrt{\lambda}}<0$. The denominator of the integrand in (6·1) has two distinct zero-points denoted by R_1 and R_2 $(>R_1)$ respectively. If $0\leqq R_0\leqq R_1$, R can not vary beyond R_1, for $I(R)$ is imaginary when $R_1<R$. But since the order of infinity at $R=R_1$ is equal to $\frac{1}{2}$, it is clear that $I(R)$ is a limited function of R. If $R_2\leqq R_0$, $I(R)$ has evidently a finite lower limit.

(c) Case: $A-\frac{2}{3\sqrt{\lambda}}=0$. The denominator of the integrand in (6·1) has a double zero-point $\frac{1}{\sqrt{\lambda}}$. If $\frac{1}{\sqrt{\lambda}}>R_0\geqq 0$ and $\frac{1}{\sqrt{\lambda}}>R\geqq 0$, it can easily be shown that $I(R)$ has a definite lower limit. If $R_0>\frac{1}{\sqrt{\lambda}}$ and $R>\frac{1}{\sqrt{\lambda}}$, then $I(R)$ can take any preassigned real value.

From these it follows that (a), (b) and the first part of (c) are

unadmissible cases and the second part of (c) is admissible by considering the physical meaning of t. In this unique zero-pressure solution, by the relation $A=\frac{2}{3\sqrt{\lambda}}$, we can perform the integration in (6·1) as follows,

$$\frac{(R-R_{-\infty})\{R+R_{-\infty}+\sqrt{R(R+2R_{-\infty})}\}^{\sqrt{3}}}{2R+R_{-\infty}+\sqrt{3}R(R+2R_{-\infty})}=Ce^{\frac{t}{R_{-\infty}}}, \qquad (6\cdot2)$$

where $R_{-\infty}$ and C represent $\frac{1}{\sqrt{\lambda}}$ and the value at $t=0$ of the left-hand side of (6·2) respectively[1].

From (6·2) and (1·1), it follows that R approaches $R_{-\infty}$ and the line-element tends to

$$ds^2=-R_{-\infty}^2(d\vartheta^2+\sin^2\vartheta d\varphi^2+\sin^2\vartheta\sin^2\varphi d\psi^2)+dt^2,$$

when t converges to $-\infty$. That is, we can say that the zero-pressure world is an Einstein's cylindrical world having $R_{-\infty}$ as its radius in an indefinitely long past. If t increases gradually from $-\infty$ to $+\infty$, R increases also from the definite value $R_{-\infty}$ to $+\infty$, as can easily be seen from (6·2). Therefore the density

$$\rho=\rho_0=\frac{2R_{-\infty}}{\varkappa R^3}$$

approaches to zero when $t\to+\infty$. According to § 5, we can conclude that our zero-pressure world will become a de Sitter's spherical one having $\sqrt{3}\,R_{-\infty}$ as its curvature radius, if the time elapses indefinitely. Since its total invariant mass remains unchanged i. e. it takes a constant value $\frac{2\pi^2R_{-\infty}}{\varkappa}$ during this process, our zero-pressure model of the universe has a somewhat different character from the actual universe in which an enormous quantity of matter is being transformed into radiating energy. But as for the red displacement of light emitted from distant objects, the explanation by this model is very satisfactory. If $R(0)$ and $R(t_1)$ are assumed to be greater than $R_{-\infty}$ in such an order that the squares of $\frac{R_{-\infty}}{R(0)}$ and $\frac{R_{-\infty}}{R(t_1)}$ can be neglected for unity, t_1 being the emitting time instant, we obtain, from (6·2),

$$\frac{R(t_1)}{R(0)}=e^{-\frac{t_1}{\sqrt{3}R_{-\infty}}}\fallingdotseq1-\frac{t_1}{\sqrt{3}\,R_{-\infty}}. \qquad (6\cdot3)$$

1. This solution was found in a different way by Lemaître. (Cf. R. C. Tolman: Proc. Nat. Acad. Sci., **16**, 582 (1930).

By (6·2) and (4·9), we get the formula

$$V=-\frac{t_1}{\sqrt{3}R_{-\infty}}, \tag{6·4}$$

which says that the Doppler shift of extragalactic nebulae is proportional to their distances, provided that their proper motions are neglected. Taking a step further, let us consider n extragalactic nebulae having equal distances from the origin. Then, by (4·8), we get

$$\frac{\Sigma V}{n}=-\frac{t_1}{\sqrt{3}R_{-\infty}}, \tag{6·5}$$

where ΣV is the sum of their radial velocities due to Doppler shift; for $\Sigma(v_r)_1$ vanishes on account of the non-existence of systematic proper motions in such a world. If we select 8 nebulae of this kind from Hubble's table[1], our estimation of $R_{-\infty}$ by means of (6·5) gives the value

$$R_{-\infty}=1.15\times 10^{27}\text{cms.} \tag{6·6}$$

Hence we get

$$M_0=\frac{2\pi^2 R_{-\infty}}{\varkappa}=1.21\times 10^{55}\ \text{gms.} \tag{6·7}$$

§ 7. Non zero-pressure solution.

When the total invariant mass is constant, we have seen that $f(R)$ is of the form

$$f(R)=D+\frac{B}{R}. \tag{3·10}$$

Here we will not consider this type of solution, since de Sitter's research[2] in 1930 corresponds to this and the annihilation of matter does not take place in such a world.

There is no ground to determine the form of $f(R)$, when M_0 depends on t. For the purpose of this determination, first let us assume that the world tends to an Einstein's cylindrical one having $R_{-\infty}$ as its radius when t decreases indefinitely, that is to say, our first assumption claims that the cosmological constant appearing in the amplified field-equations means the reciprocal of the squared radius of the Einstein's cylindrical world which was the form of our idealized actual universe at the beginning of eternity.

1. E. Hubble: Proc. Nat. Acad. Sci., **15**, 168 (1929).
2. W. de Sitter: loc. cit.

In consequence of this, if we denote

$$\Psi(x)=\frac{\lambda}{3}x^2-1+\frac{\varkappa f(x)}{3x},$$

we get, from (3·6),

$$\Psi(R_{-\infty})=0, \quad \Psi'(R_{-\infty})=0.$$

Since these are reducible to

$$\varkappa f(R_{-\infty})=2R_{-\infty}, \quad f'(R_{-\infty})=0,$$

$f(R)$ must be of the form

$$\varkappa f(R)=2R_{-\infty}+\left(\frac{1}{R_{-\infty}}-\frac{1}{R}\right)^2\Phi(R), \tag{7·1)a}$$

$\Phi(R)$ being assumed to be expanded in the series

$$\Phi(R)=a_0+a_1\left(\frac{R_{-\infty}}{R}\right)+a_2\left(\frac{R_{-\infty}}{R}\right)^2+\cdots\cdots, \tag{7·1)b}$$

which is convergent at $R=R_{-\infty}$.

Second let us assume that if t becomes infinitely great R also becomes so and the ratio $\frac{M_0}{(M_0)_{t=-\infty}}$ tends to a constant $\alpha(0\leqq\alpha<1)$, that is to say, our second assumption claims that at the end of eternity the radius of our world becomes indefinitely great and its pressure becomes zero, while its total invariant mass decreases to an amount α times as great as that of the beginning. Then $\Phi(R)$ can be put in the form

$$\Phi(R)=-2R_{-\infty}^3(1-\alpha)+a_1\left(\frac{R_{-\infty}}{R}\right)+a_2\left(\frac{R_{-\infty}}{R}\right)^2+\cdots\cdots, \tag{7·2}$$

by (3·8), (7·1)a and (7·1)b.

By (7·1)a, (7·2) and the theorem obtained in § 5, we can show that the world tends to the de Sitter's spherical one when $t\to+\infty$. In the following we shall treat the most simple case contained in it i. e. $a_1=a_2=\cdots\cdots=0$. Applying (7·1)a and (7·2) to (3·6), (3·7) and (3·8), we get

$$t=\int_{R_0}^{R}\frac{dx}{\left(\frac{1}{R_{-\infty}}-\frac{1}{x}\right)\sqrt{\frac{1}{3x}\{x^3+2R_{-\infty}x^2-2R_{-\infty}^3(1-\alpha)\}}}, \tag{7·3}$$

$$p=\frac{4R_{-\infty}^3(1-\alpha)}{3\varkappa R^4}\left(\frac{1}{R_{-\infty}}-\frac{1}{R}\right), \tag{7·4}$$

$$M_0=\frac{2\pi^2R_{-\infty}}{\varkappa}\left\{\alpha+\frac{R_{-\infty}^2}{R^2}(1-\alpha)\right\}. \tag{7·5}$$

If $R(0)$ and $R(t_1)$ are assumed to be greater than $R_{-\infty}$ in such an order that the squares of $\frac{R_{-\infty}}{R(0)}$ and $\frac{R_{-\infty}}{R(t_1)}$ can be neglected for unity, we obtain, from (7·3), the same equation as (6·3). For this reason we can give a satisfactory explanation for the linear relation between Doppler shifts and the distances of extragalactic nebulae and also obtain the value

$$R_{-\infty}=1.15\times10^{27}\text{ cms.}, \tag{6·6}$$

as can easily be seen from § 6.

Differentiating (7·5) with respect to t, we get

$$\dot{M}_0=-\frac{4\pi^2R_{-\infty}^3(1-\alpha)}{\varkappa R^3}\dot{R}, \tag{7·6}$$

where $\dot{R}$ is, of course, given by (7·3). Although, if we use these formulae (7·3), (7·4), (7·5) and (7·6), we can deduce the expression for annihilation of matter, we cannot estimate the percentage rate for annihilation owing to a wide range of values (observational) depending on the type of stars considered. Therefore we will try to estimate it for several values of α lying between $\frac{1}{10}$ and 1. In this case, by means of (7·5), (7·6) and (7·3), we get approximately

$$[\dot{M}_0]_{t=0}=\pi^2R(0)^3[\rho_0]_{t=0}=\alpha\frac{2\pi^2R_{-\infty}}{\varkappa}, \tag{7·7}$$

$$\left[-\frac{1}{M_0}\frac{dM_0}{dt}\right]_{t=0}=\frac{2(1-\alpha)R_{-\infty}}{\sqrt{3}\,\alpha R(0)^2}. \tag{7·8}$$

Using Hubble's value of density

$$[\rho_0]_{t=0}=1.5\times10^{-31}\frac{\text{gm.}}{\text{cm.}},$$

we can determine $R(0)$ by (7·7) and then estimate the percentage rate for annihilation of matter in our universe by (7·8).

For $\alpha=\frac{11}{27}$, we get $\left[-\frac{\dot{M}_0}{M_0}\right]_{t=0}=8.1\times10^{-12}\ (\text{years})^{-1}$ and $R(0)=1.5\times10^{28}$ cms. In this case, the elliptic integral in (7·3) being expressed by elementary functions only, the rate is nearly equal to that of Betelgeuse and the present radius in 13 times as great as $R_{-\infty}$.

For $a=\frac{31}{32}$, we get $\left[-\frac{\dot{M}_0}{M_0}\right]_{t=0}=1.0\times10^{-12}$ (years)$^{-1}$ and $R(0)=2\times10^{28}$ cms. This rate is just equal to that of Sirius A.

For $a=1-5.4\times10^{-4}$, we get $\left[-\frac{\dot{M}_0}{M_0}\right]_{t=0}=1.7\times10^{-15}$ (years)$^{-1}$ and $R(0)=2\times10^{28}$ cms. In this case, for which the ratio $\frac{(M_0)_{t=-\infty}-(M_0)_{t=+\infty}}{(M_0)_{t=-\infty}}$ is equal to that of electron and proton, the percentage rate is nearly twice as great as that of 60 Kruger B.

For $a=1-2.3\times10^{-4}$, we get $\left[-\frac{\dot{M}_0}{M_0}\right]_{t=0}=7.0\times10^{-16}$ (years)$^{-1}$ and $R(0)=2\times10^{28}$ cms. This value of rate is just equal to that of 60 Kruger B.

Thus we see that this non-statical universe serves as a reasonable model in many respects.

In conclusion the writer takes pleasure in thanking Prof. Tamaki for his kind advice and encouragement in the carrying out of this research.

Sur les Conditions Thermiques d'un Météorite s'approchant du Soleil d'après la Loi de la Gravitation

par

Toshima Araki et **Kiyosi Yamamura**

(Reçu le 30 janvier, 1932)

On ne doute pas à présent que la comète soit constituée des météorites enumérables. Par conséquent, pour étudier la physique de la comète on doit examiner d'abord celle de l'amas des météorites. Il nous semble ainsi intéressant d'étudier, par exemple, les conditions thermiques des météorites.

Dans ce mémoire nous avons calculé la température d'un météorite faisant un mouvement keplérien autour du soleil.

§ 1. Les équations du mouvement d'un météorite sous la gravitation solaire s'écrivent facilement, en employant les coordonnées polaires :

$$\frac{d^2r}{dt^2} - r\left(\frac{d\theta}{dt}\right)^2 + \frac{M}{r^2} = 0$$

$$r^2\frac{d\theta}{dt} = \text{cons.},$$

où M est la masse du soleil de manière que la constante de la gravitation soit égale à l'unité.

Une intégrale des équations ci-dessus est donnée par

$$\frac{dr}{dt} = -\sqrt{2M}\sqrt{\Phi(r)}. \tag{1}$$

Ici $\Phi(r)$ est une fonction de r seulement dont la forme dépend du caractère du mouvement. En effet, pour l'orbite elliptique, elle est exprimée par

$$\Phi(r) = \frac{p}{2}\left\{\left(\frac{1}{p} - \frac{1}{r_0}\right)^2 - \left(\frac{1}{p} - \frac{1}{r}\right)^2\right\}, \quad \text{(Cas 1)}$$

où r_0 et p désignent la distance de l'aphélie et le paramètre de l'orbite respectivement.

Pour l'orbite parabolique

$$(\text{Cas } 2) \qquad \Phi(r)=\frac{1}{r}\left(1-\frac{q}{r}\right),$$

q étant la distance de la périhélie.

Comme un cas spécial de celle-ci, si le météorite tombe en ligne droite au soleil de l'infinité avec sa vitesse nulle, on a

$$(\text{Cas } 3) \qquad \Phi(r)=\frac{1}{r}.$$

Dans les paragraphes suivants nous allons discuter le problème sur ces trois cas.

§ 2. Considérons à une distance r du soleil un météorite dont la forme soit une sphère de rayon R, pour simplifier le problème. Puisque le météorite n'est probablement pas un corps noir parfait, nous prenons une fraction propre ψ comme la proportion entre la chaleur absorbée et la chaleur totale acquise.

Soit T sa température absolue, ρ sa densité, C_1 sa chaleur spécifique et C_2 sa chaleur latente qui est nécessaire à faire devenir gazeuse une gramme de solide. Supposons de plus le météorite comme un conducteur parfait de la chaleur. Il ne faut pas dire que cette supposition est correcte pour le météorite de petite dimension, tandis que pour celui de la dimension grande elle n'est pas déjà exacte ; mais si le météorite a une rotation assez rapide nous pourrons la prendre comme une approximation première.

Or, écrivant l'élévation de la température et la diminution du rayon du météorite dans la durée dt avec dT et dR respectivement, nous avons immédiatement une équation suivante :

$$\frac{4}{3}\pi R^3 J C_1 \rho dT - 4\pi R^2 \cdot J C_2 \rho dR = \left(\frac{\psi S}{4\pi r^2}\pi R^2 - 4\pi R^2 \psi \sigma T^4\right)dt,$$

où S est la radiation totale du soleil par seconde, J l'équivalent dynamique de la chaleur et σ la constante de Stefan.

En tenant compte de la relation (1), cette équation deviendra

$$(2) \qquad -\frac{dT}{dr}+3\left(\frac{C_2}{C_1}\right)\frac{1}{R}\frac{dR}{dr} = \frac{3\psi}{J\sqrt{2M}\rho C_1 R}\left(\frac{S}{16\pi r^2}-\sigma T^4\right)\frac{1}{\sqrt{\Phi(r)}}.$$

Cette équation générale ne peut pas être résolue sans quelques hypothèses, car nous ne connaissons pas quelle partie de la chaleur acquise soit dissipée pour élever la température du météorite et quelle partie pour évaporer sa matière.

Nous allons ainsi simplifier le problème en considérant comme suivant :

(a) Jusqu'à ce que le météorite obtienne une température critique, par exemple le point de fusion, l'évaporation de la matière serait négligeable devant l'élévation de la température ;

(b) Après avoir atteindre cette température critique, le météorite perdrait sa matière par l'évaporation en tenant sa température constante. H. N. Russell[1] a discuté sur la diminution de la masse du météorite dans le cas 3 du paragraphe 1 dans l'occasion quand il considérait la matière de météorites au voisinage des étoiles.

§ 3. D'abord nous considérons le cas où l'évaporation de la matière est négligeable ; alors nous avons $\frac{dR}{dr}=0$ et ainsi il suit de l'équation (2),

$$\frac{dT}{dr}+\left\{\frac{A}{r^2}-\left(\frac{T}{B}\right)^4\right\}\frac{1}{\sqrt{\Phi(r)}}=0, \tag{3}$$

où

$$\begin{cases} A=\dfrac{3S}{16\pi\sqrt{2M}}\dfrac{1}{R_1}, \\ \dfrac{1}{B^4}=\dfrac{3\sigma}{\sqrt{2M}}\dfrac{1}{R_1}. \end{cases} \tag{4}$$

Ici nous appellerons provisoirement $R_1=C_1\rho R/\psi$ le "rayon effectif". C'est une constante dépendante de la dimension et des propriétés physiques du météorite. Par exemple pour le météorite de fer, R_1 est à peu près égal au rayon vrai R.

Prenons, comme l'unité de r et celle de R, le rayon du soleil et un centimètre respectivement. Alors on a

$$A=1.26\times10^6\cdot R_1^{-1}, \qquad B^4=2.16\times10^8\cdot R_1. \tag{5}$$

(i) *Cas de l'orbite circulaire* :——C'est un cas spécial de Cas 1 du paragraphe 1. Ce cas a été discuté par J. H. Poynting[2] dans l'occasion quand il calculait la température des planètes et par H. N. Russell.[3]

1 H. N. Russell : Ap. J. **69** (1929) 49.
2 J. H. Poynting : Scientific Papers, Cambridge, 1920, pp. 304—331.
3 H. N. Russell : loc. cit.

Dans ce cas, comme nous avons $r=r_0=$constante et $\Phi(r)=0$, l'équation (3) s'écrira alors

$$\frac{A}{r_0^2}-\left(\frac{T}{B}\right)^4=0 \quad \text{ou bien} \quad T=\frac{A^{1/4}B}{\sqrt{r_0}}.$$

Les résultats des calculs sont donnés dans la première colonne de la Table I. Bien que la température à la surface du soleil soit 4059° après nos calculs, ce n'est pas autre chose qu'une conséquence de notre supposition que la radiation du soleil soit acquise par l'aire πR^2 du météorite, une supposition intenable au voisinage du soleil.

(ii) *Cas 3 du paragraphe 1* :——L'équation (3) prend une forme suivante,

$$r\sqrt{r}\,\frac{dT}{dr}+A-\left(\frac{T\sqrt{r}}{B}\right)^4=0. \tag{6}$$

On peut obtenir facilement la solution générale de cette équation différentielle, mais cela n'a pas de sens en pratique. Il suffit pour notre but d'obtenir une solution particulière qui satisfait à la condition initiale, c'est-à-dire $T=0$ pour $r=\infty$.

Une telle est donnée par la solution singulière

$$T=\frac{\mathfrak{T}}{\sqrt{r}} \tag{7}$$

où $\mathfrak{T}$ est une racine positive de l'équation du 4^e degré suivante,

$$\mathfrak{T}^4+\frac{B^4}{2}\mathfrak{T}-AB^4=0. \tag{8}$$

En effet cette équation algébrique a une racine positive dans l'intervalle $0<\mathfrak{T}<2A$. En introduisant les valeurs A et B de (5), nous pouvons calculer $\mathfrak{T}$ pour quelques valeurs de R_1.

On voit les résultats dans la première ligne de la Table I.

Avec ces valeurs de $\mathfrak{T}$ l'équation (7) donne la température cherchée du météorite pour la distance donnée r du soleil, comme la Table I montre. Il va sans dire que pour $R_1=0$ les températures correspondent à celles dans le cas de l'orbite circulaire.

(iii) *Cas 2 de* § 1 (*L'orbite parabolique*) :——L'équation fondamentale est

$$r\sqrt{r}\sqrt{1-\frac{q}{r}}\,\frac{dT}{dr}+A-\left(\frac{T\sqrt{r}}{B}\right)^4=0. \tag{9}$$

Table I

$r/R_\odot$ \ R_1 (mètre)	0	1	5	10	20	30	50	100	500	1000
1	4059°	3890°	3190°	2270°	1250°	830°	500°	250°	53°	27°
2	2871	2751	2256	1605	884	587	354	177	37	19
4	2030	1945	1595	1135	625	415	250	125	27	14
9	1353	1297	1063	757	417	277	167	83	18	9
16	1015	973	798	568	313	208	125	63	13	7
25	812	778	638	454	250	166	100	50	11	5
36	677	648	532	378	208	138	83	42	9	4.5
49	580	556	456	324	179	119	71	36	8	4.0
64	508	486	399	284	156	104	62	31	7	3.4
81	451	432	354	252	139	92	56	28	6	3.0
100	406	389	319	227	125	83	50	25	5	2.7

Il est clair que la solution de cette équation différentielle est développable en série des puissances de $\frac{q}{r}$.

Puisque l'équation (9) ne diffère de (6) que le facteur $\sqrt{1-\frac{q}{r}}$, le premier terme de cette série est nécessairement égal à $\frac{\mathfrak{T}}{\sqrt{r}}$. En effet la forme de cette solution peut être écrite comme il suit,

$$T=\frac{1}{\sqrt{r}}\left(\mathfrak{T}+\mathfrak{T}_1\frac{q}{r}+\mathfrak{T}_2\left(\frac{q}{r}\right)^2+\ldots\ldots+\mathfrak{T}_n\left(\frac{q}{r}\right)^n+\ldots\ldots\right).$$

Les coefficients $\mathfrak{T}_1$, $\mathfrak{T}_2$,.....sont déterminés par introduire cette expression dans l'équation (9). Nous les avons calculés pour $R_1=100$, 1000 et 10000 cm ; ils se trouvent dans la Table II.

Table II

R_1	100 cm.	1000 cm.	10000 cm.
$\mathfrak{T}$	3890°	2270°	250°
$\mathfrak{T}_1$	78.3	330.5	41.7
$\mathfrak{T}_2$	20.6	137.7	18.8
$\mathfrak{T}_3$	10.2	78.1	11.1
$\mathfrak{T}_4$	6.4	51.0	7.5
$\mathfrak{T}_5$	4.5	36.9	5.5

Avec ces coefficients nous avons obtenu finalement les Tables IIIa, IIIb et IIIc, qui représentent les températures pour quelques valeurs de q.

Table III a ($R_1 = 100$ cm.)

q \ $r/R_\odot$	400	225	100	81	64	49	36	25	16	9	4	2	1
0	195°	259°	389°	432°	486°	556°	648°	778°	973°	1297°	1945°	2751°	3890°
0.5	195	259	389	432	486	556	648	778	974	1298	1950	2765	3936
1	195	259	389	432	486	556	648	779	974	1300	1956	2784	4010
2	195	259	389	432	486	556	649	779	975	1303	1967	2856	
9	195	259	390	433	487	558	651	784	985	1336			
16	195	259	390	434	489	560	654	788	1003				
25	196	261	394	438	494	566	663	802					

Table III b ($R_1 = 1000$ cm.)

q \ $r/R_\odot$	400	225	100	81	64	49	36	25	16	9	4	2	1
0	114	151	227	252	284	324	378	454	568	757	1135	1605	2270
0.5	114	151	227	252	284	324	379	455	571	763	1156	1669	2484
1	114	151	227	252	285	325	380	457	573	769	1180	1753	2904
2	114	151	228	253	286	326	381	459	579	784	1230	2053	
9	114	152	230	256	290	333	392	482	627	967			
16	114	152	232	259	294	339	406	509	726				
25	118	159	248	280	320	375	455	581					

Table III c ($R_1 = 10000$ cm.)

q \ $r/R_\odot$	400	225	100	81	64	49	36	25	16	9	4	2	1
0	13	17	25	28	31	36	42	50	63	83	125	177	250
0.5	13	17	25	28	31	36	42	50	63	84	128	184	278
1	13	17	25	28	31	36	42	50	64	85	131	196	335
2	13	17	25	28	31	36	42	51	64	87	138	237	
9	13	17	25	28	32	37	43	53	69	111			
16	13	17	26	29	32	38	45	55	74				
25	13	18	28	32	36	42	52	67					

(iv) *Cas* 1 *du paragraphe* 1 (*L'orbite elliptique*) :——Il n'est pas facile d'obtenir la solution dans ce cas. Mais puisque nous avons déjà traité les orbites circulaire et parabolique, nous nous contenterons dans ce cas général de calculer la limite supérieure de la température du météorite ; cette limite T' est donnée immédiatement, en négligeant le terme $\left(\frac{T}{B}\right)^4$ dans l'équation (3) :

$$\frac{dT'}{dr}+\frac{A}{r^2\sqrt{\Phi(r)}}=0$$

où

$$\Phi(r)=\frac{1}{r}-\frac{1}{r_0}-\frac{p}{2}\left(\frac{1}{r^2}-\frac{1}{r_0^2}\right).$$

L'intégrale de cette équation est

$$T'=\frac{A}{\sqrt{\frac{p}{2}}}\arcsin\frac{1-\frac{p}{r}}{1-\frac{p}{r_0}}+\text{cons.}$$

§ 4. Dans les paragraphes précédants nous avons supposé que l'évaporation de la matière de la surface soit négligeable.

Nous traiterons ici du cas où l'élévation de la température du météorite est négligeable, la chaleur acquise étant toute dissipée pour l'évaporation. Ce sera peut-être correct après que le météorite a atteint une certaine température critique T_1 s'approchant du soleil. Alors $\frac{dT}{dr}=0$ et en posant $R_2=C_2\rho R/\psi$ l'équation fondamentale (2) deviendra

$$\frac{dR_2}{dr}=\left(\frac{\alpha}{r^2}-\beta\right)\frac{1}{\sqrt{\Phi(r)}} \tag{10}$$

où

$$\alpha=\frac{S}{16\pi J\sqrt{2M}}=4.19\times10^5$$
$$\beta=\frac{\sigma}{J\sqrt{2M}}T_1^4=1.54\times10^{-9}T_1^4 \tag{11}$$

dans le même système des unités que celui de (4).

La solution de l'équation différentielle (10) est très facilement obtenue, à savoir :
pour l'orbite elliptique (Cas 1)

$$\text{Cons.}-R_2=\alpha\sqrt{\frac{2}{p}}\arcsin\left(\frac{\frac{1}{p}-\frac{1}{r}}{\frac{1}{p}-\frac{1}{r_0}}\right) \tag{12}$$
$$+\frac{\beta\sqrt{2p}r_0^2}{2r_0-p}\,r\sqrt{\left(\frac{1}{p}-\frac{1}{r_0}\right)^2-\left(\frac{1}{p}-\frac{1}{r}\right)^2}$$

$$+\frac{\beta_1\sqrt{2}\,r_0^3}{(2r_0-p)^{2/3}}\arcsin\frac{\frac{r}{a}-1}{e};$$

pour l'orbite parabolique (Cas 2)

$$(13)\qquad \text{Cons.}-R_2=\frac{2a}{\sqrt{q}}\theta+\frac{2\beta q\sqrt{q}}{3}(3\cot\theta-\cot^3\theta)$$

où

$$\frac{q}{r}=\sin\theta;$$

et enfin pour Cas 3 du paragraphe 1

$$(14)\qquad \text{Cons.}-R_2=\frac{2a}{\sqrt{r}}+\frac{2}{3}\beta r\sqrt{r}.$$

§ 5. Quand on veut appliquer les résultats des paragraphes précédents, on ne peut pas éviter de rencontrer quelques difficultés pratiques.

En effet nous n'avons pas non seulement les connaissances suffisantes sur les matières qui constituent la comète, mais encore il y a plusieurs matières dont la chaleur de la fusion et celle de l'évaporation ne sont pas connues. Mais il nous semble possible que du moins nous considérions qualitativement par notre théorie les conditions thermiques de la comète considérée comme l'amas des météorites, en s'appuyant sur quelques supposition plausibles.

(1) D'abord nous allons constater les conclusions de nos discussions des paragraphes précédents sur un météorite qui tombe au soleil,—à part de la comète. Provisoirement supposons que le météorite soit de fer. Puisque la densité et la chaleur spécifique de fer sont entre 7.0—7.9 et 0.08—0.15 respectivement, $R_1=C_1\rho R/\psi$ donne approximativement le rayon vrai du météorite. Or le point de fusion et celui d'ébullition du fer sont à 1800° et 3272° abs. respectivement.

Nous pouvons ainsi constater par les résultats de § 3 (i) que les météorites de fer, quelque soient ses dimensions, ne peuvent pas survivre en écrivant une orbite circulaire à l'éloignement moins grand que 4-fois de rayon solaire : il faut qu'ils aient été tout évaporés depuis déjà bien longtemps.

Pour une distance donnée du soleil, le météorite acquiert la température la plus basse dans le Cas 3, où il tombe en ligne droite de l'infinité au soleil. Dans ce cas les résultats de § 3 (ii) nous permettent de constater que le météorite de fer avec un diamètre au-dessus de 5 mètres

peut arriver à la surface du soleil sans évaporation. Avec un diamètre au-dessous de cette valeur il s'annulerait en chemin. Si l'on considère un peu plus généralement le cas de l'orbite parabolique, d'après § 3 (iii) on voit qu'il n'y a pas de météorite avec le rayon de 1 mètre quand il a une distance de la périhélie moins grande que $2R_\odot$.

Quant aux autres matières nous pouvons poursuivre les discussions similaires.

(2) Les comètes du groupe de Jupiter ont déjà tourné plusieurs fois autour du soleil jusqu'aujourd'hui depuis qu'elles avaient été capturées par Jupiter. Dans telles comètes les météorites avec la température de fusion très basse se seraient tout annulés en évaporation.

Notre théorie permet de donner quelques considérations numériques de tel phénomène. La diminution Δm de la masse m d'un météorite correspondante à celle du rayon effectif ΔR_2, est donnée par l'inégalité suivante :

$$\frac{\Delta R_2}{R_2} < \frac{\Delta m}{m} < \frac{3\Delta R_2}{R_2}.$$

Prenons comme un exemple la comète d'Encke (q=0.3, e=0.9). Considérons les météorites de la matière ordinaire dont la température critique est entre 350° et 150° absolument mesurée. La distance r qu'ils font telle température est calculée par § 3 (iv) et ensuite ΔR_2 se trouve, d'après (12), de l'ordre de 10^4—10^5 cm. pendant une révolution. Puisque $R_2 = C_2\rho R/\psi$, la chaleur latente C_2 est de l'ordre de 10^2 et la densité ρ de l'ordre de 10 pour plusieurs matières, tous les météorites de telle matière s'annuleraient dans les révolutions pendant des milliers ou dizaines de milliers d'années. En conséquence les comètes considérées comme appartenantes aujourd'hui à Jupiter ne sont entièrement composées que des météorites tels que ceux de fer ou de pierre dont la température critique est trés haute.

(3) Si l'éclat absolu de la comète est déterminé seulement par les conditions géométriques, il doit être en proportion réciproque à la 2^e puissance de la distance du soleil. Mais en pratique son éclat est en proportion à r^{-s}, où $s>2$, au lieu de r^{-2}.

Par exemple l'éclat de la grande comète en 1910 janvier[1] était proportionnel à $r^{-4.6}$. La distance de la périhélie de cette comète est à peu près égale à 28 $R_\odot$. En appliquant les valeurs de T pour $q = 25\ R_\odot$ et $R_1 = 10000$ cm. dans la Table III c, on trouve que T se varie

1. S. Orlow: A. N. **189**, pp. 1—6.

avec $r^{-0.58}$ approximativement. Si l'on peut supposer que l'éclat de la comète dépende indirectement, en quelque façon, de la température de ses météorites, celle-ci exerçant une influence sur la luminosité du gazeux qui remplit la comète et de plus que la loi de cette dépendence soit T^4, alors son éclat sera en proportion à $r^{-4.3}$. Cet accord avec des observations serait bien attribué à l'accident, car la cause de la luminescence cométaire n'est pas tellement simple.

Les matières constitutives de la comète sont diverses. Ainsi elles commenceraient à évaporer graduellement selon sa température critique, suivant que la comète s'approche du soleil, en devenant la queue et le coma. Par conséquent, quand nos connaissances sur les composants de la comète seront accrues par l'étude spéctroscopique etc., il y aura une possibilité d'appliquer notre théorie à l'étude de la physique cométaire.

Vol. XV, No. 2, Published March 30, 1932

Price - - - - Yen 1.80

These Memoirs are on Sale at

MARUZEN COMPANY, LTD.
TOKYO, OSAKA, KYOTO, NAGOYA, YOKOHAMA,
FUKUOKA & SEND I

昭和七年三月二十五日印刷
昭和七年三月三十日發行

編纂兼發行者　京都帝國大學理學部

印刷者　須磨勘兵衛
京都市下京區北小路通新町西

印刷所　內外出版印刷株式會社
京都市下京區西洞院七條南

賣捌所　丸善株式會社
東京、大阪、京都、名古屋、横濱、福岡、仙臺

CONTENTS

On the Origin of the X-Ray Non-Diagram Lines in the *K* Series
By Masao Sawada 43

Biochemical Study on the Autumn Fall of the Leaf
By Shigeru Komatsu and Shinsaku Ozawa 57

The Diffusion of Zinc in Copper and its Alloys
By Yoshito Yamauchi 67

On the Solutions of the Cosmological Field Equations and Some Models of the Universe with Annihilation of Matter
By Shūjiro Kunii 97

Sur les Conditions Thermiques d'un Météorite s'approchant du Soleil d'après la Loi de la Gravitation
Par Toshima Araki et Kiyosi Yamamura 113